1961

Thermal buckling of a thin ring heated on the inner periphery

Mathews, Donald William

Stanford University

THERMAL BUCKLING OF A THIN RING HEATED ON THE INNER PERIPHERY

A THESIS
SUBMITTED TO THE DEPARTMENT OF AERONAUTICAL ENGINEERING
AND THE COMMITTEE ON THE GRADUATE DIVISION
OF STANFORD UNIVERSITY
IN PARTIAL FULFILLMENT OF THE REQUIREMENTS
FOR THE DEGREE OF
ENGINEER

By
Donald William Mathews
August 1961

ACKNOWLEDGMENT

The research described in this thesis was part of a general investigation conducted by the Department of Aeronautical Engineering at Stanford University and was sponsored by the United States Air Force Office of Scientific Research, Contract No. AF 49(638)223.

The author wishes to express his profound appreciation to Professor W. H. Horton for his invaluable and timely suggestions in all phases of this investigation.

The writer is also deeply indebted to the Stanford University Photography Department for their untiring assistance.

TABLE OF CONTENTS

LIST OF ILLUSTRATIONS

LIST OF ILLUSTRATIONS (Cont'd)

LIST OF TABLES

NOTATION

u, v, w	Components of displacement
r, θ	Polar coordinates
a	Inner radius of disc
b	Outer radius of disc
ρ	r/b
μ	a/b
h	Thickness of disc
E	Modulus of elasticity in tension
ν	Poisson's ratio
c	Coefficient of thermal expansion
$D = Eh^3/12(1-\nu^2)$	Flexural rigidity of plates and shells
T	Temperature rise above initial state
T_o	Temperature rise above initial state at $r = a$
ϵ_r, ϵ_θ	Unit elongation in radial and tangential directions
σ_r, σ_θ	Radial and tangential normal stresses in polar coordinates
M	Bending moment per unit length
q	Specific load normal to undeflected disc
$\cdot$	$\frac{\partial w}{\partial r}$
$k = \frac{cT_o(b^2 - a^2)}{h^2(1-\nu^2)}$	Non-dimensional buckling coefficient

t	Time
$H = \frac{\sigma_r}{T_o \alpha E}$	Stress parameter
$Q = c\delta h \int rTdr$	Heat energy

I. INTRODUCTION

Design engineers, spurred by the continuous demand for a better and more efficient product, constantly face new and varied problems. Among these, those arising from heat are of increasing significance. For example, modern electric motors have become smaller and more powerful units. This has resulted in higher operating temperatures. Likewise, in the modern airplane, the need to reduce drag has caused closer cowling of engines. The need to operate in severe weather conditions has added problems of hot gas ducts and the increase in over-all speed has brought problems of kinetic heating. All these design features have introduced new problems of thermal stress for the designer. These problems arise in the following manner. When a material or structure is subjected to a temperature gradient, or when a composite structure consisting of two or more materials is heated uniformly, or non-uniformly, the various fibres tend to expand different amounts according to their respective temperatures and coefficients of expansion. Since the structure is continuous, the individual fibres are not free to expand individually and hence constrain each other. These constraints give rise to thermal stresses, the magnitude of which, depends on the temperature levels and the mechanical and physical properties of the material. Thermal stress can produce structural collapse in two ways: (1) by material failure, (2) by inducing instability. Buckling is a most important consideration in design since it can give rise to sudden and unexpected structural collapse.

Now it is the hard fact of engineering reality, that a theory is only valid if it can be practically substantiated. Therefore, the purpose of this paper is to report an investigation of the buckling behavior of a thin circular ring heated along its inner edge. Data on temperature distribution, buckling time and mode are presented, and this information correlated to determine a buckling parameter. Both fixed and free edge conditions are considered.

II. APPARATUS AND INSTRUMENTATION

2.1 Basic Experiment

As a thin disc is subjected to a thermal gradient, a stress distribution is formed. When the stresses reach a certain critical value, buckling occurs and the plate is deflected from its original shape. It was the purpose of this investigation to perform a set of tests to determine if experimental results agree with theoretical calculations. The experiments were conducted on a family of thin annular plates with the outer edge both clamped and free.

2.2 Details of the Test Specimen

To insure a plain stress condition, the plate thickness must be small enough to prevent a stress gradient across it.[1] Also a thinner plate is more consistent with the assumption of no gravity forces. However, when the thickness is too small, it is difficult to maintain an initially flat plate. From these considerations, the choice of material was 0.032 in. Alzac* and 0.074 cold roll steel. Two complete sets of rings were tested, each set being of a different material and consisting of three plates with a fixed outer edge and free inner edge, and three completely free plates. The inner radius of all test specimens was one and one-eighth inches in order to accommodate the heating source. The Moire Method (see Appendix I) was used to determine buckling. Thus a mirror-like finish was required on the surface of each plate. The Alzac had a high mirror finish and the steel was nickel plated. Typical test specimens are shown in Fig.1. A representative base and locking ring are shown in Fig.2. For the free edge condition, the outer one inch of the test plate radius rested freely on the base ring. In the fixed edge case, the locking ring clamped the outer one inch to the base. Thus the effective radius in this case was one inch less than the actual radius of the specimen.

---

* Super pure aluminum electro-polished and anodized.

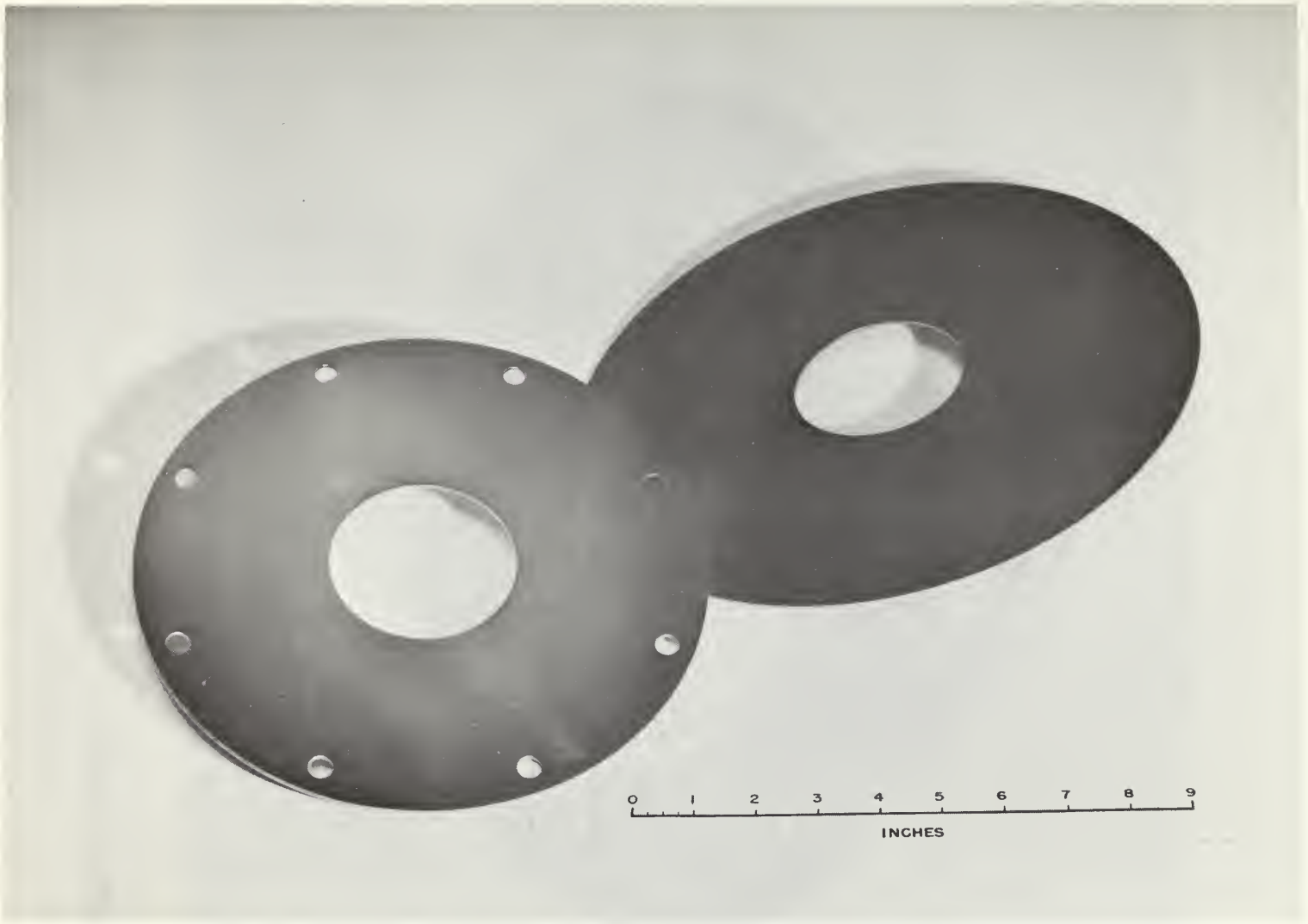

Fig.1 TYPICAL TEST PLATES

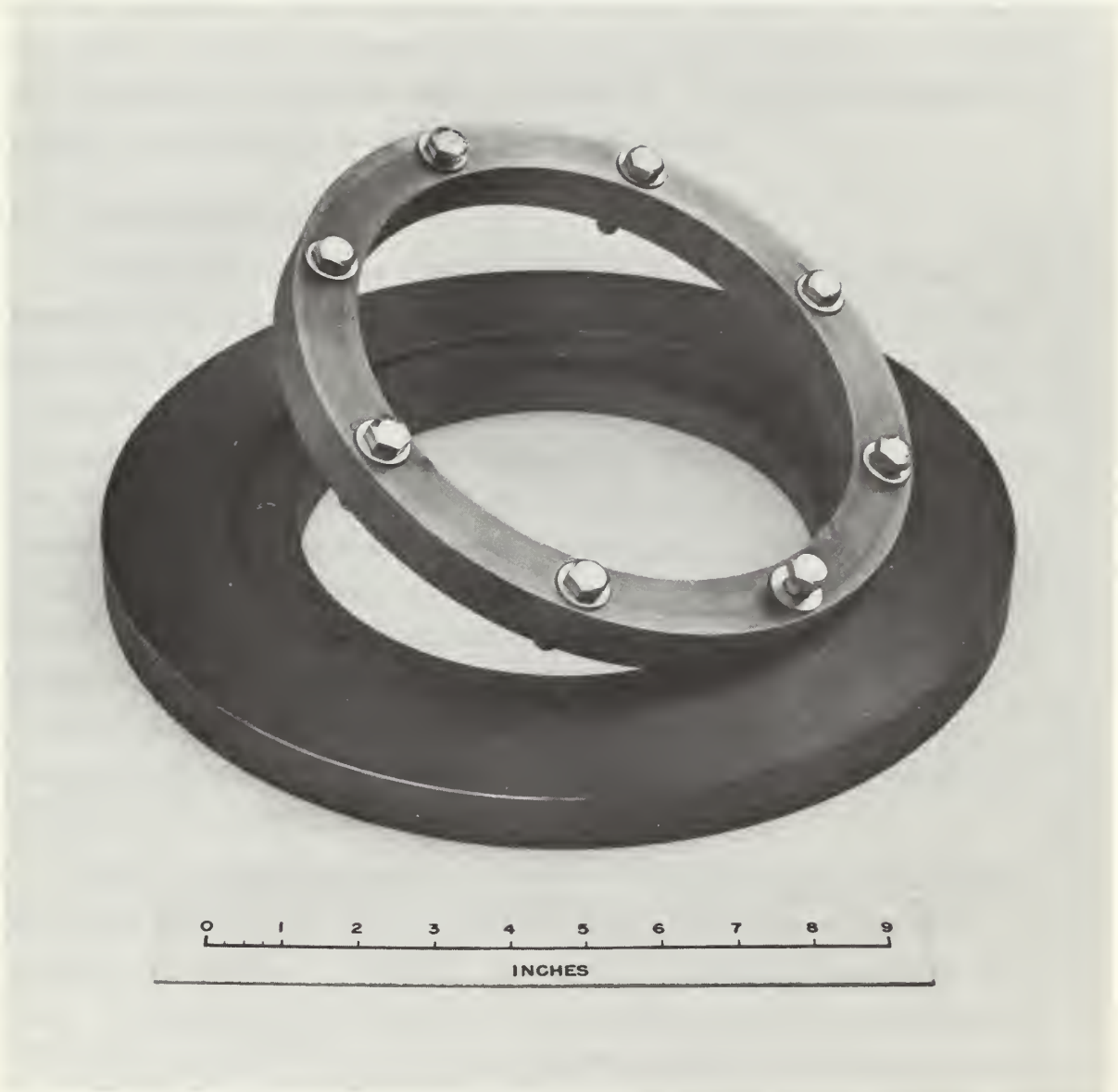

Fig.2 TYPICAL MOUNTING RING

2.3 Method of Heating

After careful consideration, the heater shown in Fig.3 was adopted and consists of three resistance wire elements. The middle loop is centered approximately one thirty-second of an inch from the inner edge of the specimen. The remaining two loops are located above and below the edge. An oven is formed by the heater jacket and acts to stabilize the temperature around the inner pheriphery. In Fig.4 the heater is shown in position for a typical fixed edge test.

2.4 Temperature Survey

A capacity discharge welder was used to make chromel-alumel thermocouples and to attach them to the test specimens. It was very difficult to weld the transducers to aluminum; however, after much experimenting, it was found that a successful bond could be made when the welding current was passed through the chromel wire to the plate. The thermal emf's were recorded on a Consolidated Engineering Corporation Recording Oscillograph , type 5-101B, with a room temperature reference junction. The oscillograph galvanometers were calibrated using a Leeds and Northrup Portable Potentiometer, and had sensitivities of the order two inches per millivolt. The response time of the recorder was well within the limits of the experiment. Thermocouple location is indicated in Fig.5, and a typical oscillograph record is shown in Fig.6.

While checking transducer accuracy it was found that convective air currents from the slide projector cooling fan caused erratic temperature readings. This was corrected by ducting the exhaust air away. Experiments also revealed that radiation from the open face of the oven caused heat to flow down the thermocouple leads to the reference junction, thus causing a false indication of plate temperature. On the inner edge the erroneous value of temperature rise was almost twice the actual value. This was corrected by mixing finely ground fire clay with Duco SR-4 cement and forming a protective bead around the thermocouple. Fire clay powder was carefully packed around the transducer after the exposed thermal junction was welded to the specimen thus completing the insulation.

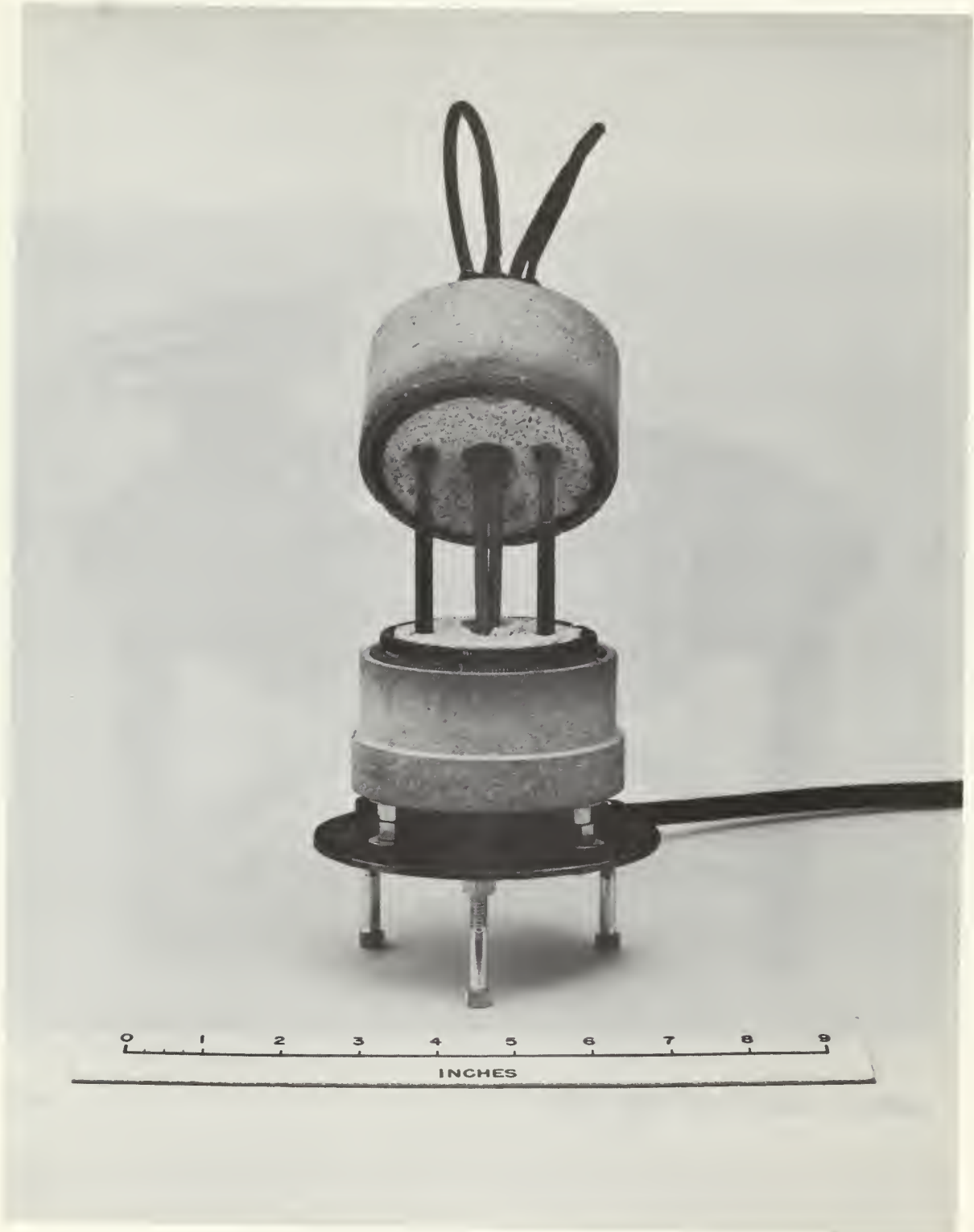

Fig.3 HEATER UNIT

Fig.4 FIXED EDGE TEST PLATE ASSEMBLY

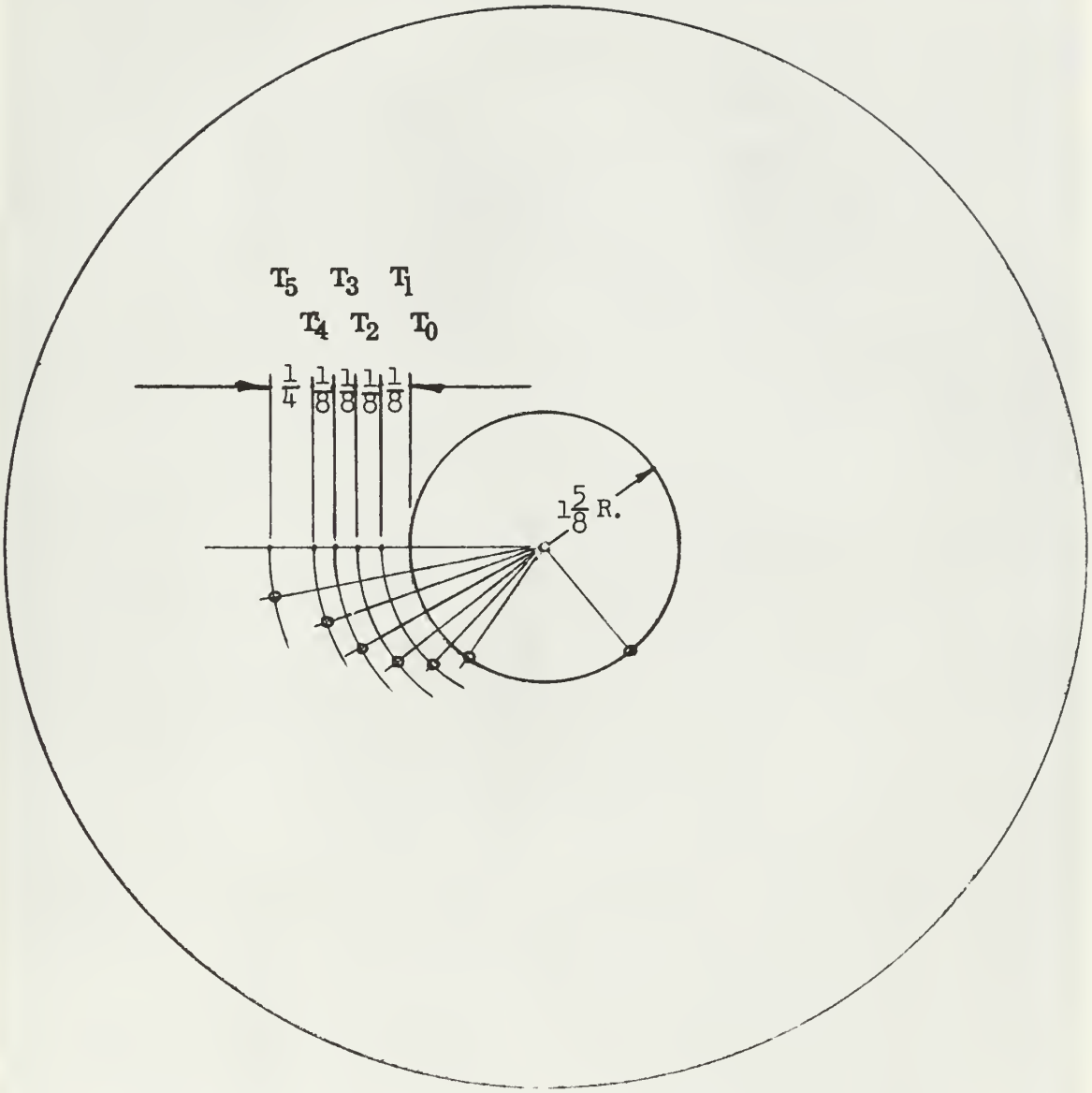

Fig. 5 THERMOCOUPLE LOCATION

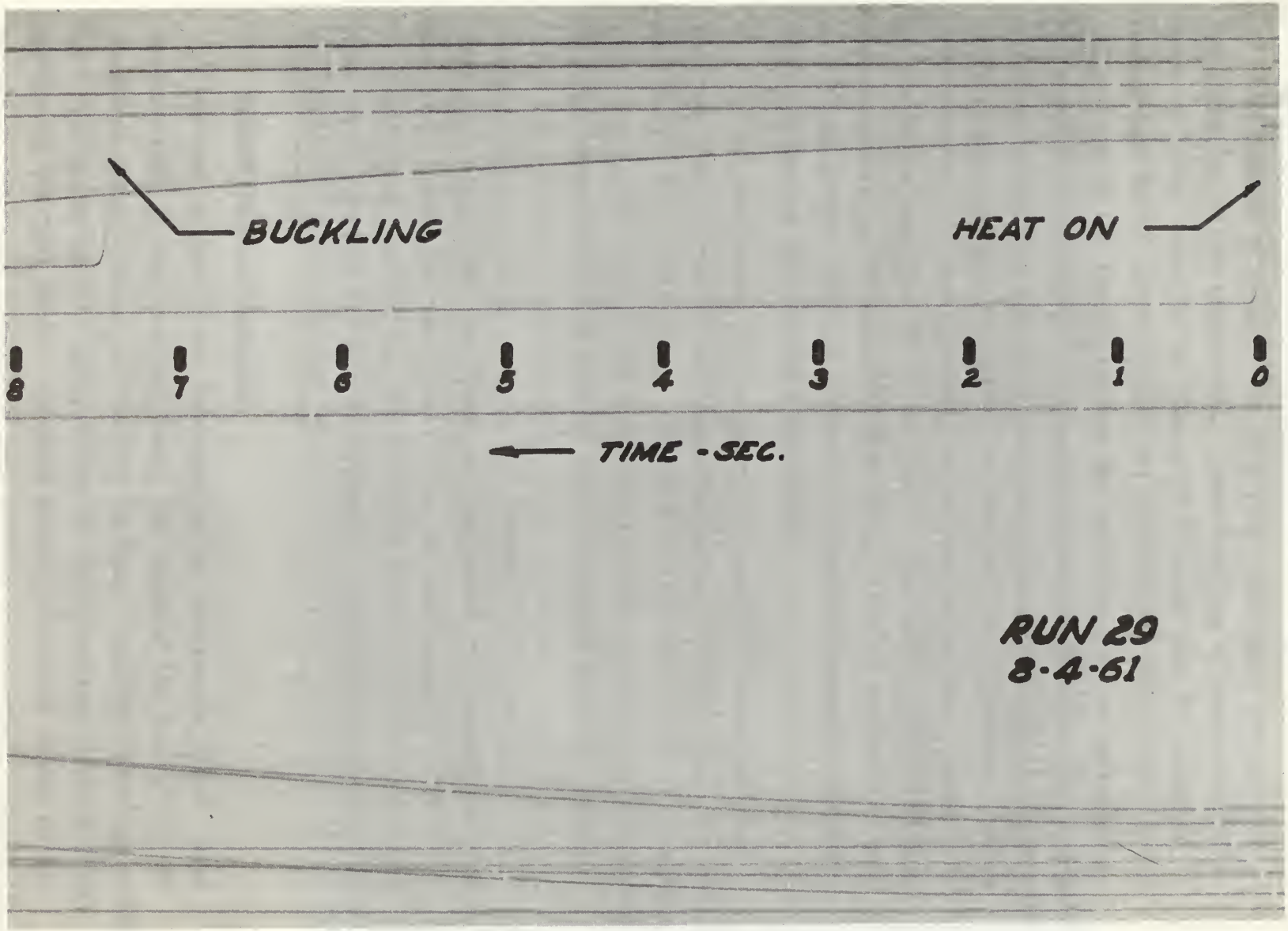

Fig.6 TYPICAL OSCILLOGRAPH RECORD

2.5 Development of Buckling Observation Technique

The essence of experiments involving buckling is the accurate determination of its occurrence. Since buckling of plates is influenced by loads normal to its plane, it is clear that the means of measurement should not influence the experiment. Even a small interaction between the transducer and the plate would alter appreciably the results of the tests.[2] In planning this experiment careful consideration was given to a number of different transducers; but the resultant study showed that whether they be of the variable reluctance, linear potentiometer, or capacity type, an interaction existed. Admittedly, in the latter case the effect was small. However, optical techniques clearly provide no interaction whatsoever. Thus it was decided that an optical method should be adopted. After some research, the Moire Method described in Appendix I was chosen.

In the development of the method it generally became apparent that there were a number of added advantages. In particular, the method gave such a fine inspection procedure that only the very best specimens were used in the study. The great power of the technique is illustrated in Fig.7 where the fringe pattern from a rejected specimen clearly shows two dimples of approximately 0.002 in. depth. The inspection procedure was also used to check the flatness of the mounting ring surfaces. Again, the sensitivity of the method was illustrated when a slope of 0.0005 in. was found on the one inch mounting surface of the twelve inch base plate. In this case irregular patterns occurred when a test specimen was bolted in place. Subsequent machining removed the slope.

2.6 Determination of Buckling

The test apparatus and instrumentation is shown in Fig.8. From the back side of the focusing plate, the image of the test plate and the Moire fringe pattern are clearly visible. Specific reference points were located on the milk glass screen by first focusing a colored line pattern on the test plate. Physical points on an axis normal to the projected lines were referenced with respect to individual colored lines.

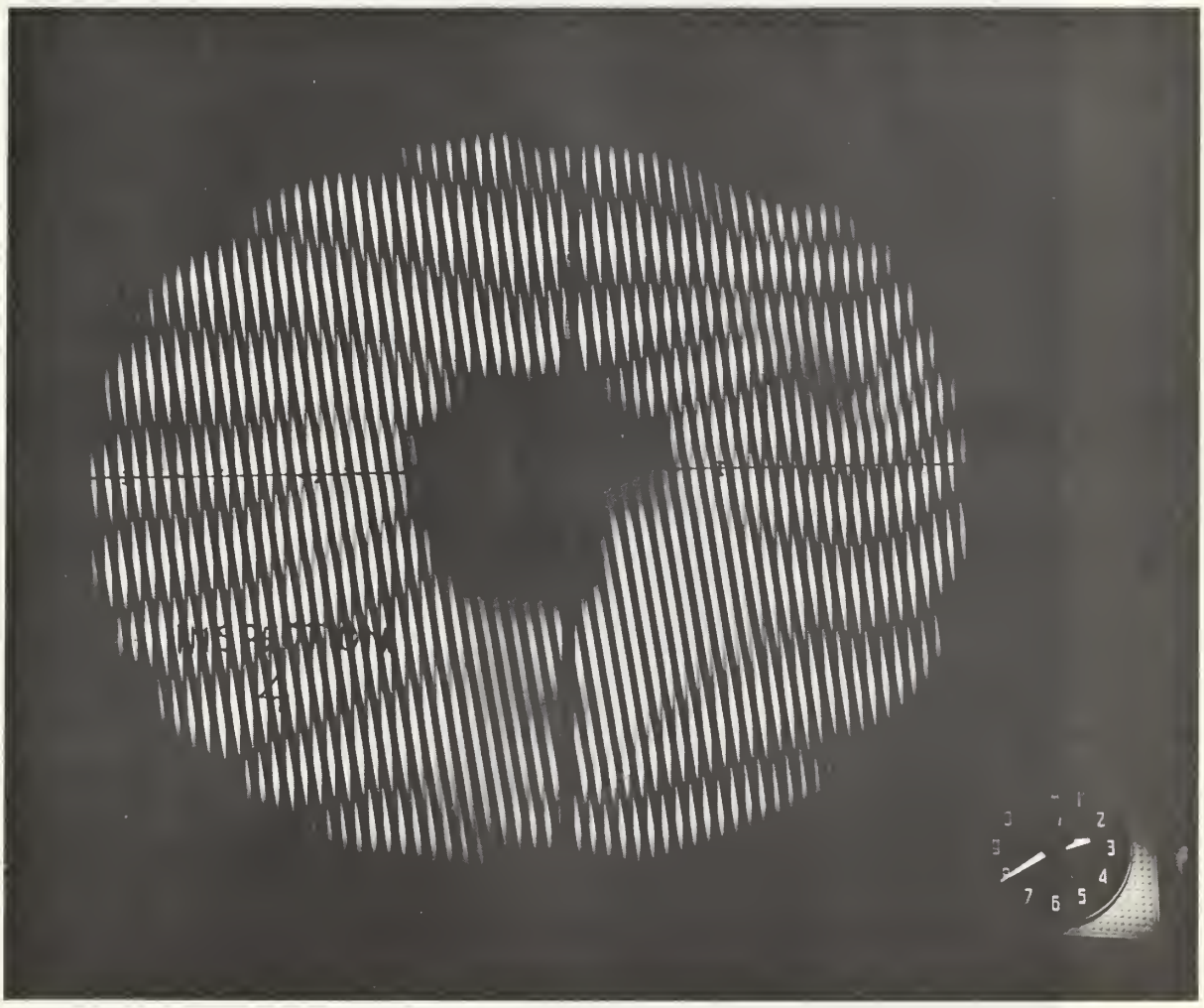

Fig.7 REJECTED TEST PLATE DURING INSPECTION

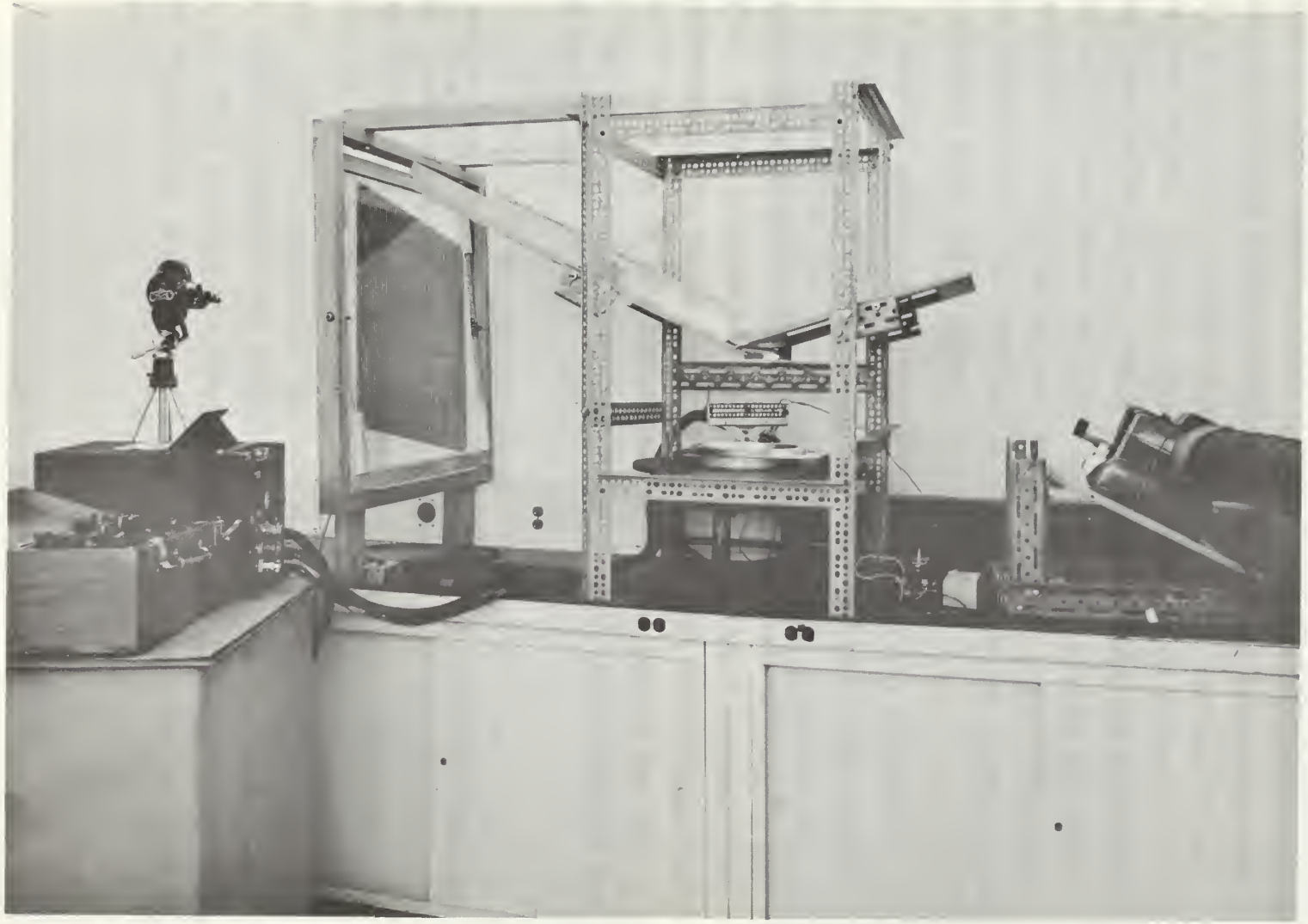

Fig.8 BUCKLING MEASURING EQUIPMENT AND INSTRUMENTATION

The projected line pattern was then refocused on the milk glass screen and in this way the corresponding coordinate points were determined. A black and white slide was used for the actual testing because it gave better contrast and fringe definition. The optical system was such that a slide could be changed without changing the position of the coordinate points. However, since their position is defined relative to any given set of lines , when the test plate moves the coordinate points change position on the focusing plate. To account for this, the movement of the fringe at any given coordinate point is measured as the ordinate from the intersection of the fringe and an appropriate line from the fixed set of lines.

A vertical scale and an electric clock with sweep second hand were placed in the viewing field of the focusing plate. One channel of the oscillographic recorder was used for a pulse indication of buckling time with the pulsing circuit triggered mechanically by the observer. Fringe movement was recorded on 16 mm Tri-X reversal film at approximately ten frames per second. A Bell and Howell camera with a 1:2.0/16 lens and f8 lens opening was used. The setting was two stops less than indicated by a light meter to give better contrast and fringe definition.

It was found that an observer could consistently detect buckling of a twelve inch outer diameter disc when the inner edge was deflected between one-half and one one-thousandth of an inch. It is relatively easy to detect when a moving object comes to rest, but exceedingly difficult to determine when motion starts, particularly if acceleration is slow. Therefore, projecting the film record in reverse made the job of checking buckling time relatively simple. The fringe patterns before and after buckling are shown in Figs. 9 and 10 respectively. The mode of buckling was determined by a qualitative inspection of the fringe pattern.

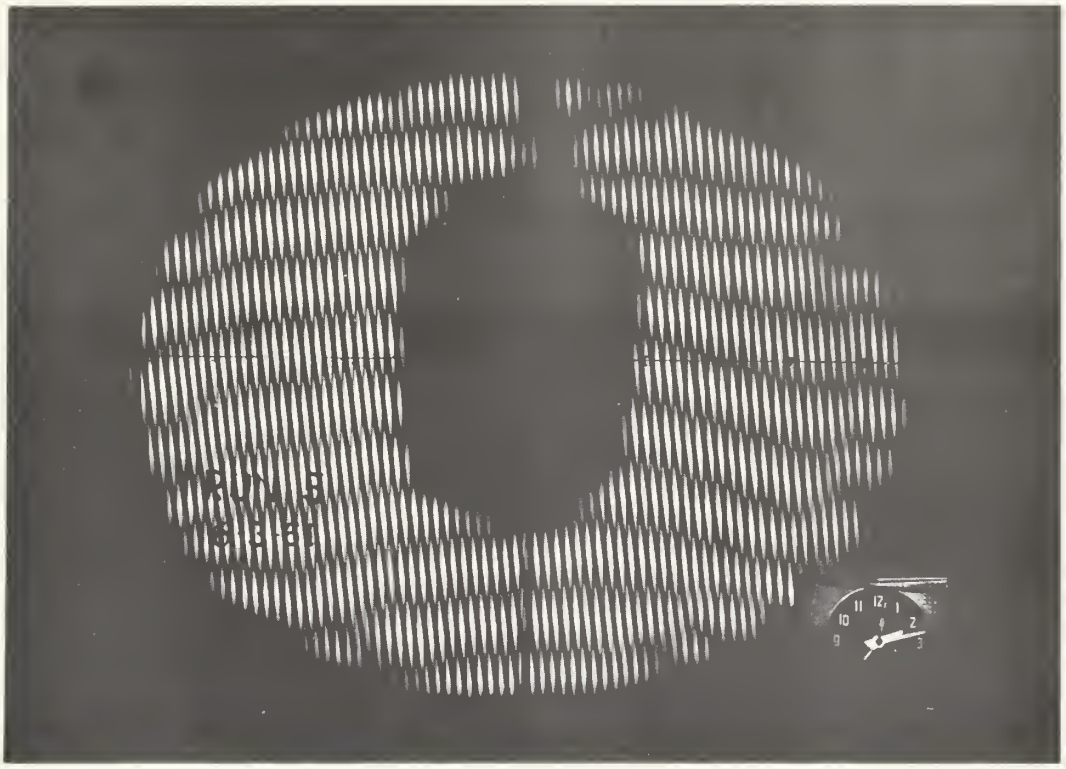

Fig.9 FRINGE PATTERN BEFORE BUCKLING

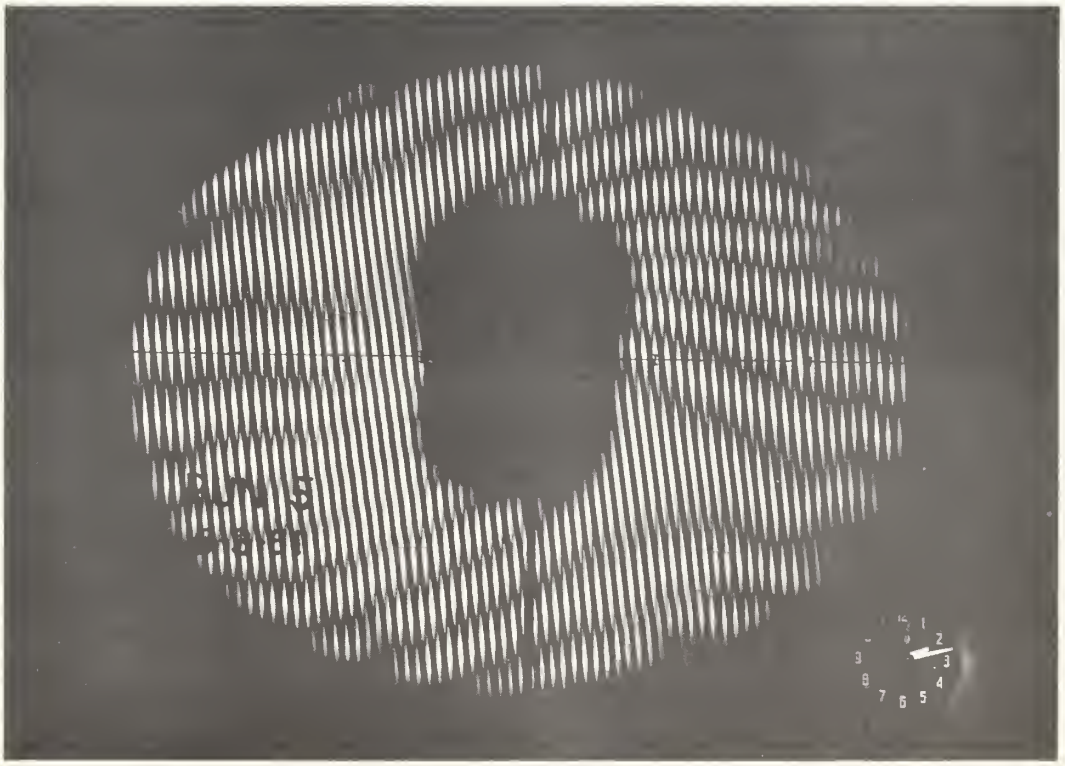

Fig.10 FRINGE PATTERN AFTER BUCKLING

III. TESTING PROCEDURE

3.1 Scope

A twelve inch outer diameter annulus was used in the initial testing to correlate the experiment. The a/b ratio of 0.271 was about mid range for the corresponding isothermal buckling parameter k and provided a physical size that was compatible with heater and optical system. The family of test specimens was then chosen to give the maximum range of $\mu = a/b$ within the physical limits of the apparatus. By varying the outer diameter from 18 in. to 8 1/8 in., the span of μ was from 0.203 to 0.406. The testing schedule is shown in Table I.

3.2 Accumulation of Data

The first five runs were not used because convective currents caused variance in rate of heating and consequently the temperature. After eliminating the air currents, runs 6, 7 and 8 were used to qualitatively determine the influence of heating rate on buckling time. A variable resistance was put into the heater circuit thus reducing heater power. Half and one-third power approximately doubled and tripled the respective buckling times. It was found that reduced power lengthened the time to such an extent that the most rigid (eight inch steel plate with fixed edge condition) specimen would not buckle in a reasonable time. Therefore, full power was used in the remaining tests. The next nineteen runs were used to check accuracy, repeatability, and radial symmetry of the temperature profile. The problem of radiation effects on thermocouples (see Section 2.4) was corrected and the resulting temperature distribution accurately described the actual values. For run 28, the three thermocouples located on the inner edge 120° apart, gave a resultant temperature distribution consistent to within one-half a degree or 0.015 millivolts. The preliminary testing having been completed, the actual runs to compile experimental data started with run 29.

A total of twenty-nine runs were made on the twelve inch alzac specimen with free outer edge. Throughout these tests the buckling time remained at about seven seconds. Thus the stress distribution at

TABLE I

SCHEDULE OF TEST RUNS

Outer radius (in.)	8		6		5		$4\frac{1}{16}$	
Effective radius b (in.)	7		6		5		$4\frac{1}{16}$	
Outer edge condition	Fix		Free		Fix		Free	
Material	Al.*	St.+	Al.	St.	Al.	St.	Al.	St.
Preliminary	1-5							
Variable power	6-8							
Uniformity	9-28							
Data	41	42	29	33	30	31	34	36
Outer radius (in.)	5		$4\frac{1}{16}$					
Effective radius b (in.)	4		$4\frac{1}{16}$					
Outer edge condition	Fix		Free					
Material	Al.	St.	Al.	St.				
Data	38	39	37	40				

* Alzac

\+ Steel

buckling remained constant. In buckling tests on circular cylinders, Holmes [3] found that the buckling load decreased after repeated testing. No such effect was evidenced in these tests. Furthermore, the inspection procedure used eliminated the possibility of very small permanent deformations occurring that might lead to this type of result.

The buckling mode remained constant with a radially symmetric dish shape. In eight runs the plate buckled up and in three the plate buckled down. Run 34 provided an example of "oil can" or "snap-through" buckling. The inner edge of the ten inch free annulus started to buckle up, approximately 0.001 in., then snapped through to a buckled down position of about 0.010 in. There were two readily apparent solutions for this phenomenon:

(1) The thermocouples were located in the top surface of the annulus and physical contact with the heater jacket could be made when the deflection was upward. The resulting vertical load provided the energy to cause the snap-through. However, in other cases of upward buckling this did not occur.

(2) All specimens tested were inspected critically and only the best were accepted. However, this specimen had a very small irregularity near the inner edge in the area of highest thermal stress. This may have given rise to bending moments which caused the phenomenon.

3.3 Experimental Results

Experimental results are given in Table II. Sample calculations for run 29 are given in Appendix II. A non-dimensional plot of temperature distribution at buckling is given in Fig.11. This has the general form of a rectangular hyperbola. Figures 12a and 12b show the stress distribution for the free and fixed edge condition respectively. It is noted that for the free edge case the annulus becomes less rigid with increasing outer diameter and for the fixed edge case there is an intermediate ring for which the rigidity is a minimum. For smaller

TABLE II

DATA AND RESULTS

Run No.	Material	Boundary Condition	E $\times 10^{-6}$	α $\times 10^{6}$	ν	a	b	$\mu = a/b$	h	t	Mode
			psi	1/°F		in.	in.		in.	sec	
40	ST	FR	30	6.1	0.25	1.625	4.0625	0.400	0.074	120.0	1
37	AL	FR	10	12.8	0.33	1.625	4.0625	0.400	0.032	12.2	1
36	ST	FR	30	6.1	0.25	1.625	5	0.325	0.074	55.3	1
**34	AL	FR	10	12.8	0.33	1.625	5	0.325	0.032	13.0	1
33	ST	FR	30	6.1	0.25	1.625	6	0.271	0.074	33.2	1
39	AL	FR	10	12.8	0.33	1.625	6	0.271	0.032	8.2	1
42	ST	FX	30	6.1	0.25	1.625	7	0.232	0.074	40.6	1
41	AL	FX	10	12.8	0.33	1.625	7	0.232	0.032	8.2	1
31	ST	FX	30	6.1	0.25	1.625	5	0.325	0.074	42.8	1
30	AL	FX	10	12.8	0.33	1.625	5	0.325	0.032	7.2	1
35	ST	FX	30	6.1	0.25	1.625	4	0.407	0.074	71.9	1
38	AL	FX	10	12.8	0.33	1.625	4	0.407	0.032	9.7	1

** Snap-through Buckling case

TABLE II (Continued)

Run No.	T_o +	T_o +	T_o ++	T_1	T_2	T_3	T_4	T_5	$H_{max} \times 10^2$	$\sigma_{r\ max}$	$(\rho)\sigma_{r\ max}$	k	$Q \times 10^4$
	°F	°F	°F	°F	°F	°F	°F	°F		psi			btu
40	292	320	320	227	157½	107	79½	57	8.50	4960	0.510	5.27	5740
37	40½	24	33	17	5½	3	2½	1	5.45	230	0.460	6.50	61
36	252½*	190½	230	167	48½	35½	24½	16½	5.95	2500	0.405	6.10	2145
34	43½	34	44	19	6	2	1	0	3.05	265	0.385	13.85	42
33	131*	184½*	182	52	33½	13	13½	5½	4.55	1500	0.320	7.20	1083
29	12½	10½	12	3½	1	1	1	-	4.80	74	0.315	5.68	15
42	114½	88	121	59	29	20½	19	12½	7.55	1665	0.300	6.65	1150
41	7	8½	8½	2½	0	0	0	0	4.45	48	0.265	5.53	9
31	246*	174	200	90	48	31	18	13½	7.50	2750	0.410	5.30	1648
30	15	15	15	3½	½	½	0	0	4.12	79	0.375	4.77	15
39	342½*	236½*	300	147	75½	58	38	26	8.82	4820	0.560	4.78	3060
38	26½	19	28	6½	2½	1	½	½	4.50	161	0.482	5.23	30

+ Thermocouple values not corrected for slight differences in location

++ Critical temperature at r = a from temperature profile curves

* Estimated

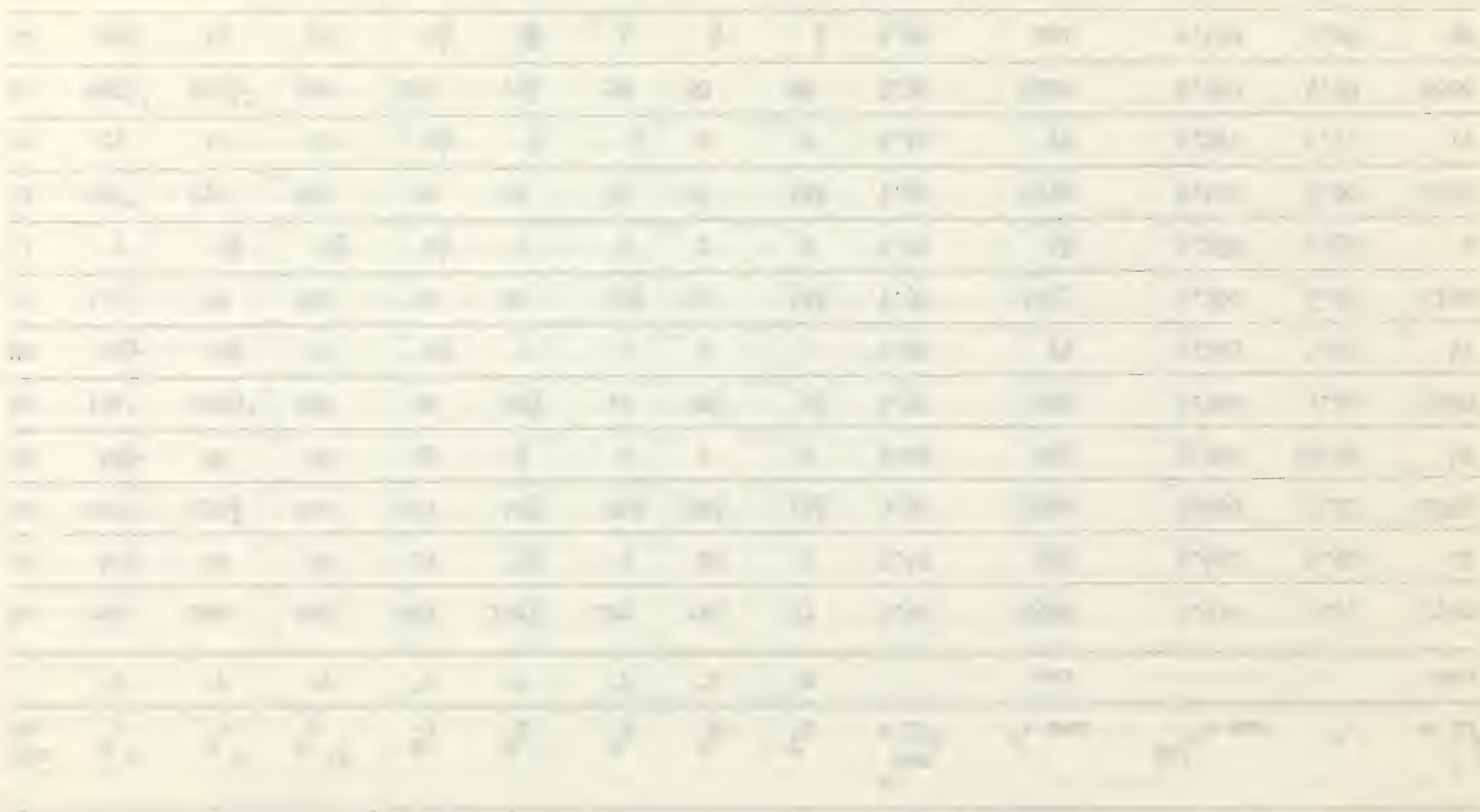

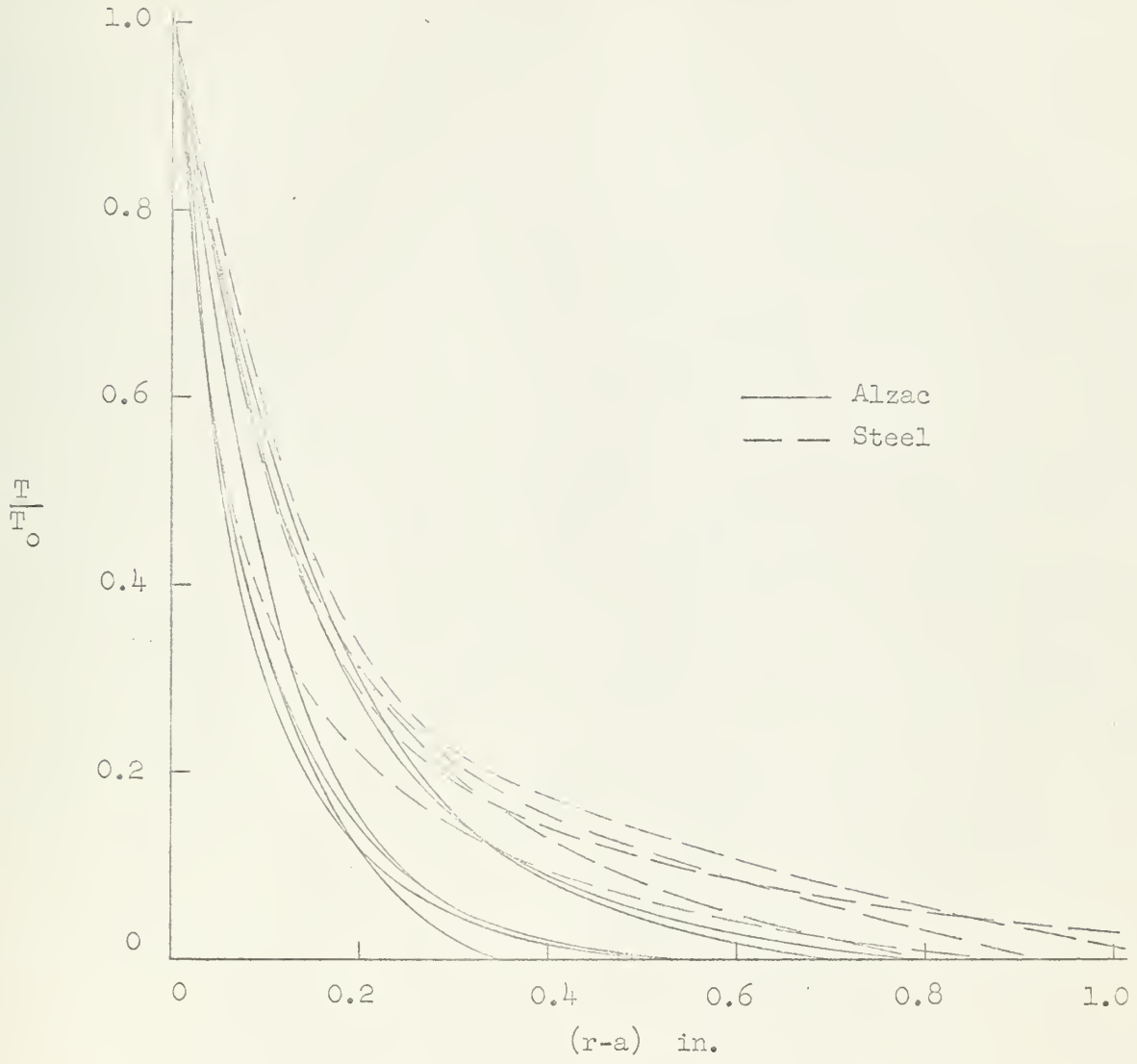

Fig. 11 NON-DIMENSIONAL TEMPERATURE DISTRIBUTION AT BUCKLING

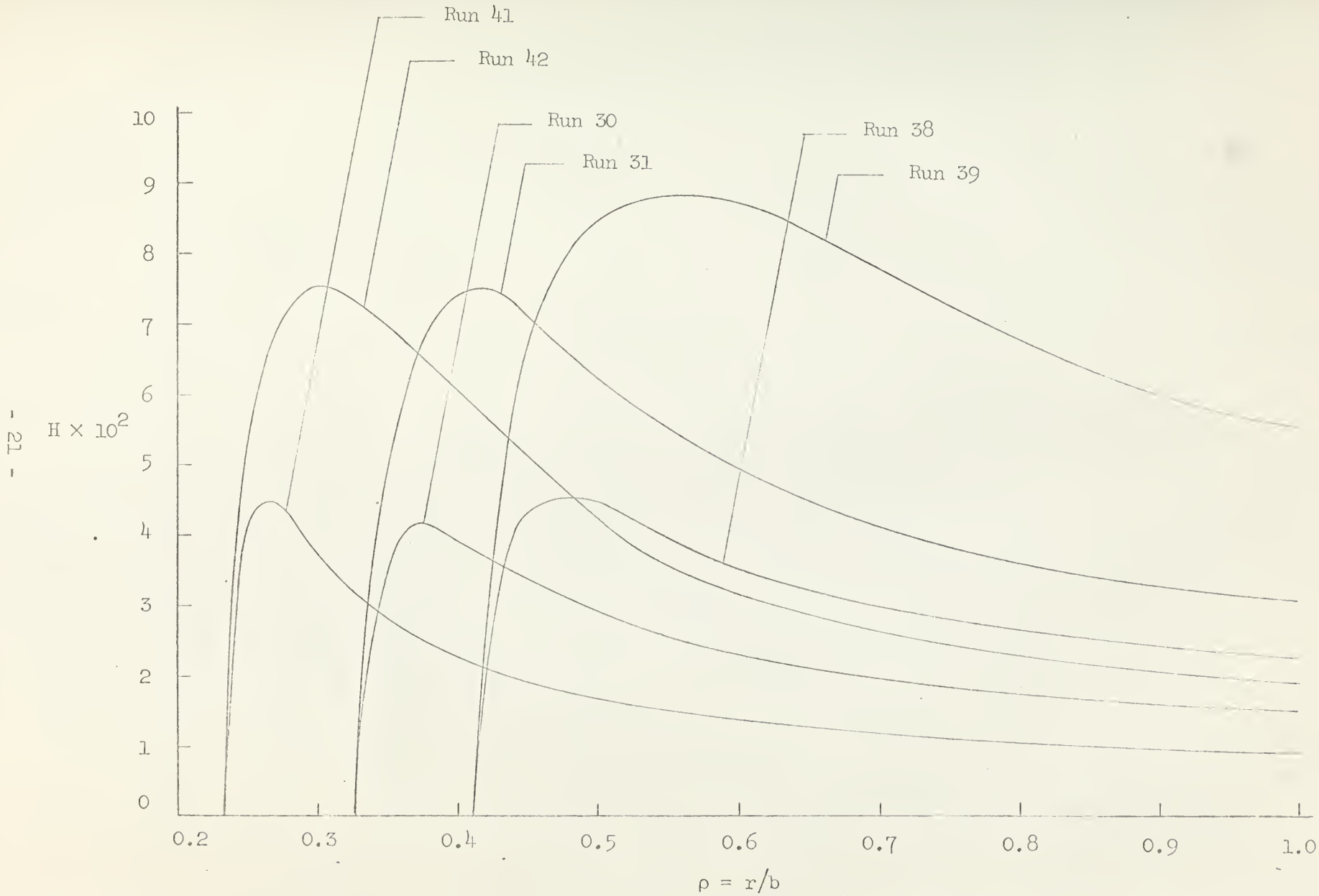

Fig. 12a

FIXED EDGE RADIAL STRESS DISTRIBUTION

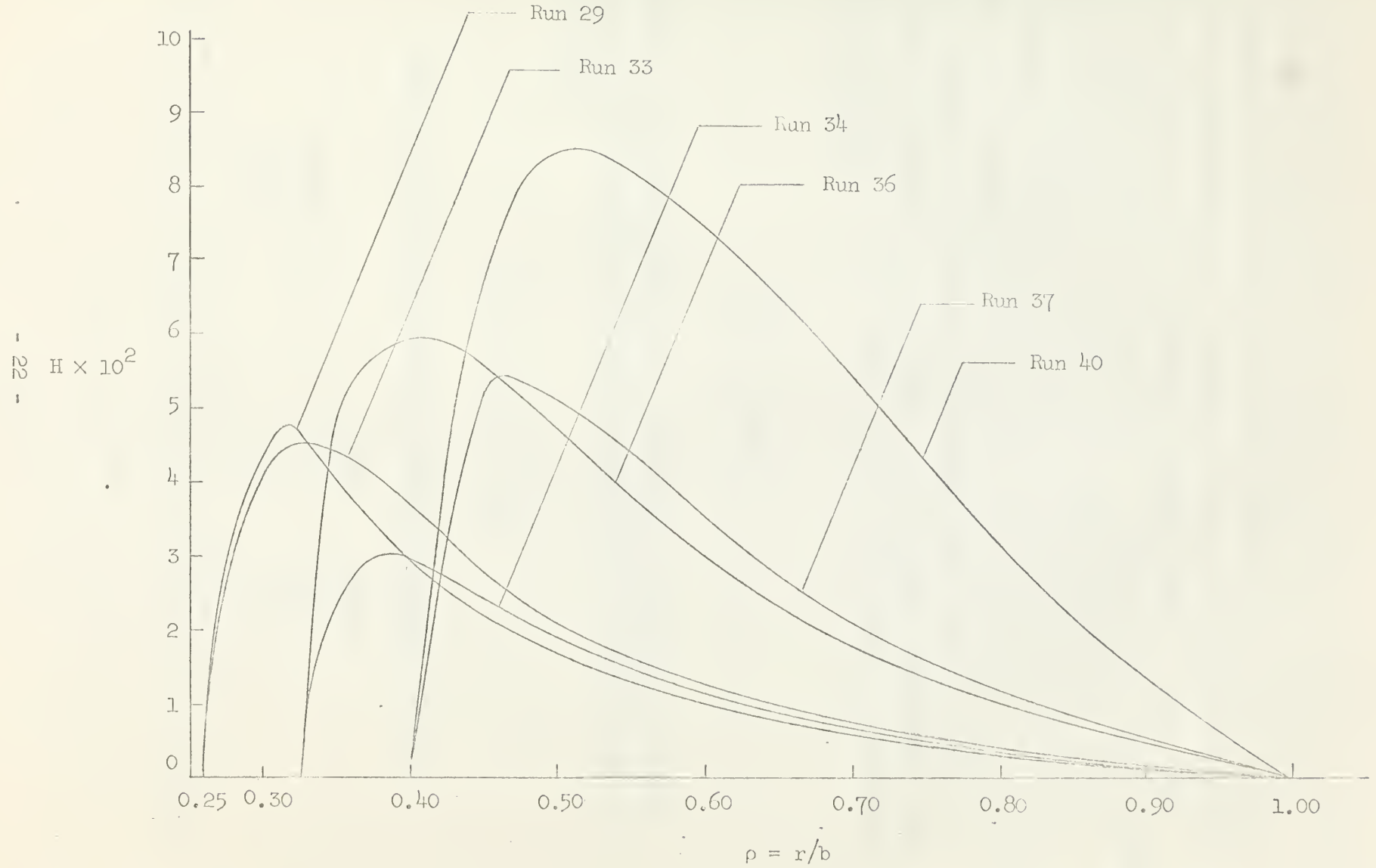

Fig. 12b

FREE EDGE RADIAL STRESS DISTRIBUTION

outer diameters the fixed edge condition stiffens the ring and for larger diameters the limiting case is a plate without a hole. The buckling parameters for both fixed and free edge conditions are given in Figures 13a and 13b respectively. The general trend of the buckling parameters is the same as in the corresponding isothermal case of a ring loaded with uniform pressure at the outer edge.[6] However, on the thermal problem, the fixed edge case is in general, less rigid than the free. This is due to the compressive load developed along the fixed edge during the application of thermal loading. These buckling forces tend to neutralize the normal stiffening effect of the fixed edge, and in fact, overcome it completely. Experimental evidence shows that at buckling both the critical temperature T_o and time t have a simple relationship with the heat energy Q stored within the plate. The general expression for heat energy is

$$Q(t) = \int_V Tc\delta \, dV$$

where c is specific heat and δ the density. Hence for an annular plate with axi-symmetric temperature distribution constant across the thickness

$$Q(t) = 2\pi c\delta h \int_a^b Tr dr$$

Assuming the following nominal values for physical constants:

	Steel	Alzac
Specific heat c	0.12	0.21
Density δ	0.285	0.10

the heat energy at buckling was calculated. Critical temperature is shown in Fig.14 as a function of heat energy, and has the relationship

$$T_o = 2.95 \, Q^{0.564}$$

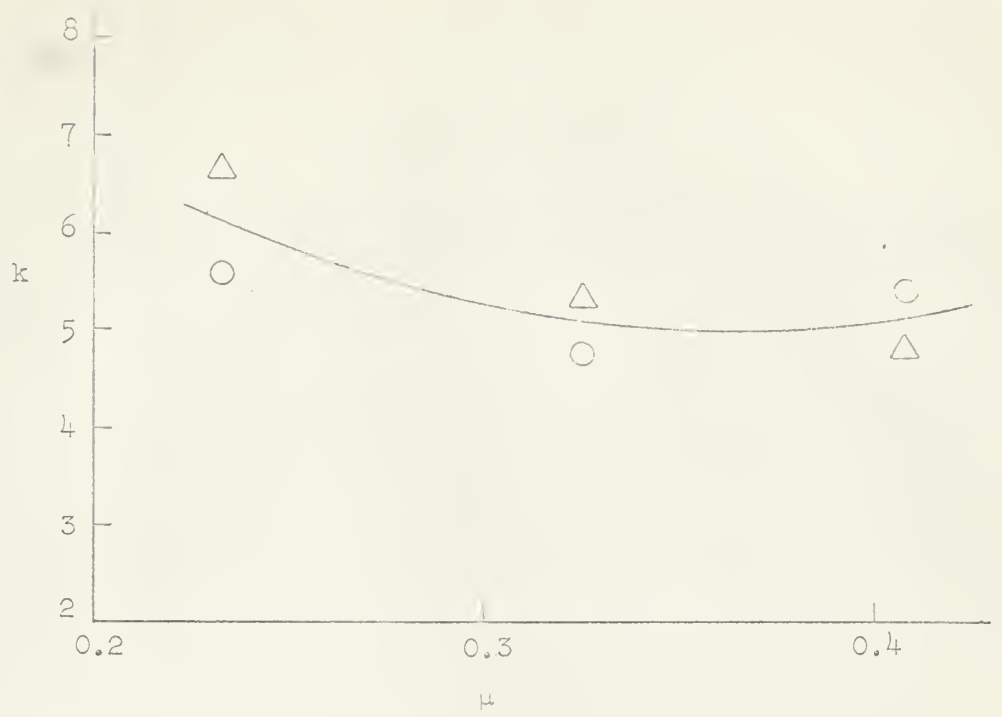

Fig. 13a FIXED EDGE BUCKLING COEFFICIENT

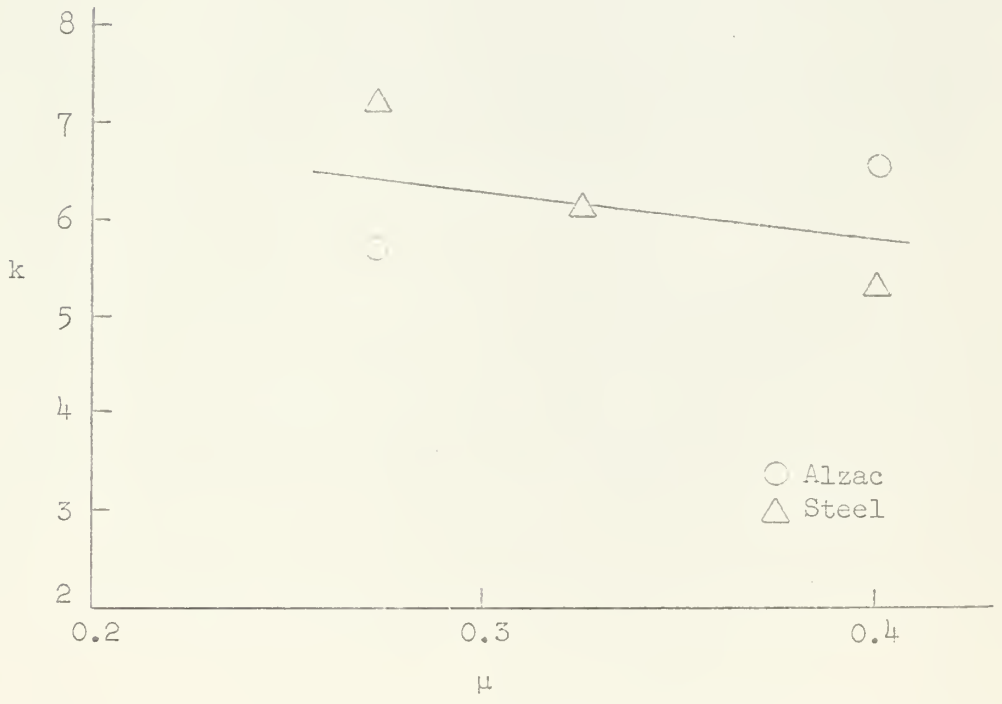

Fig. 13b FREE EDGE BUCKLING COEFFICIENT

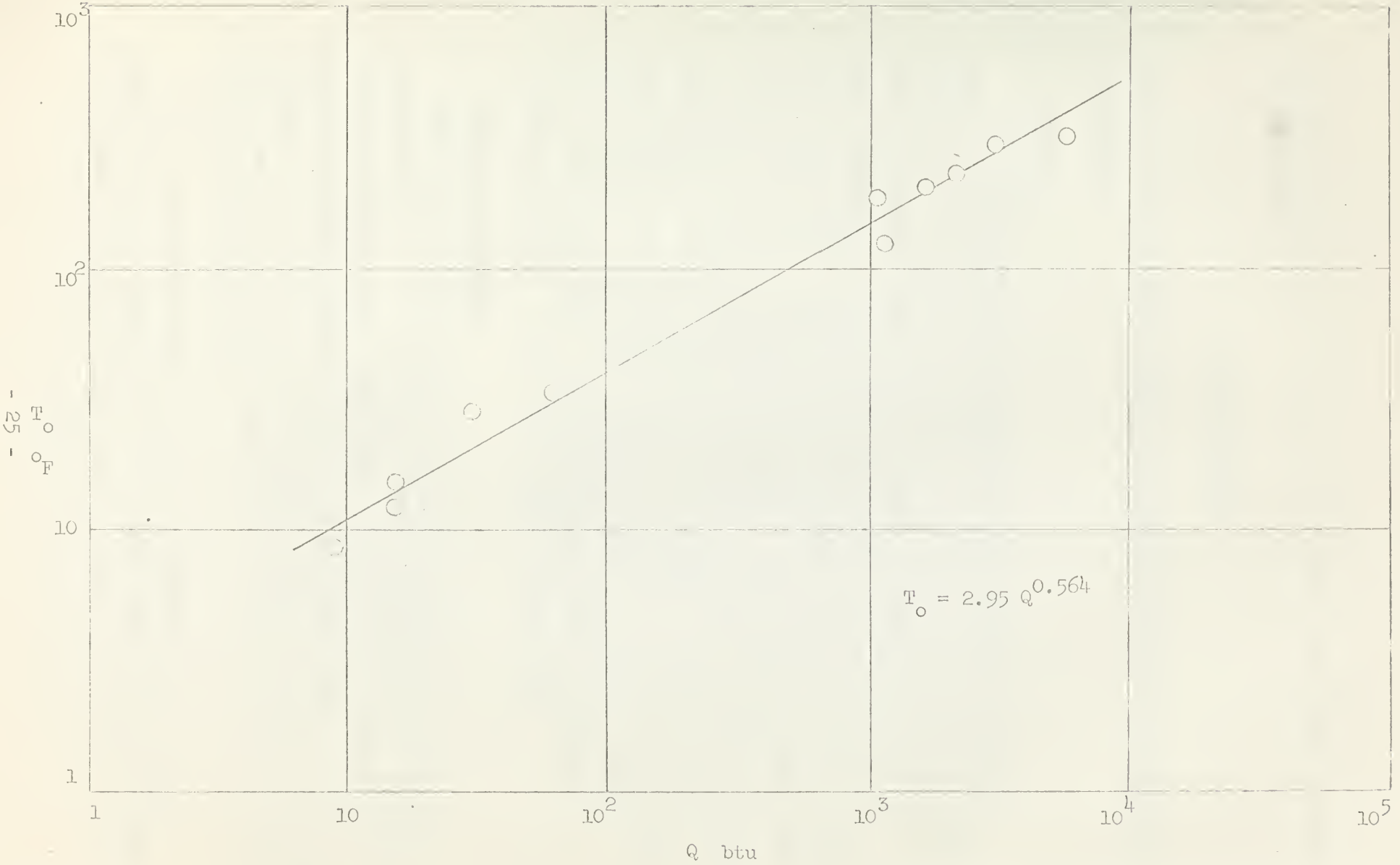

Fig. 14 HEAT ENERGY - CRITICAL TEMPERATURE RELATION

In Fig.15 buckling time is shown as a function of heat energy and has the relationship

$$t = 0.233\ Q^{0.404}$$

With these relationships critical temperature and time of buckling can be predicted.

3.4 Accuracy

For chromel-alumel thermocouples the emf generated is of the magnitude 0.02 millivolts per degree. Because of the extremely small voltages and the inherent variables in the associated measuring equipment, the measured temperature is accurate to approximately half a degree fahrenheit. Almost immediately after heat was applied to the inner edge, a small indication of temperature rise was observed on the galvanometer trace. The indication then remained almost constant until the actual temperature gradient developed. These fluctuations of up to a degree in magnitude were attributed to external sources other than temperature, and were neglected in the analysis. Buckling times and temperatures were consistent except for run 34, in which occurred snap-through buckling. This had a critical time and temperature almost double the expected value. The experimental scatter in values of buckling coefficient k was of the order $\pm$ 10 per cent.

3.5 Extension of Tests

The range of results could be extended to cover both larger and smaller values of μ. In the latter case the limiting value represents the plate without a hole. Practically this could be accomplished by decreasing the inner radius and using the same type heater. A delay in buckling is to be expected. On the other hand, an increase in hole radius should also cause an increase in rigidity for the fixed edge case and a decrease for the free plate.

As μ approaches unity there is a transition from the annulus problem to one of a thin strip. If the outer edge is fixed, the tangential stresses will cause buckling along the free edge similar to that

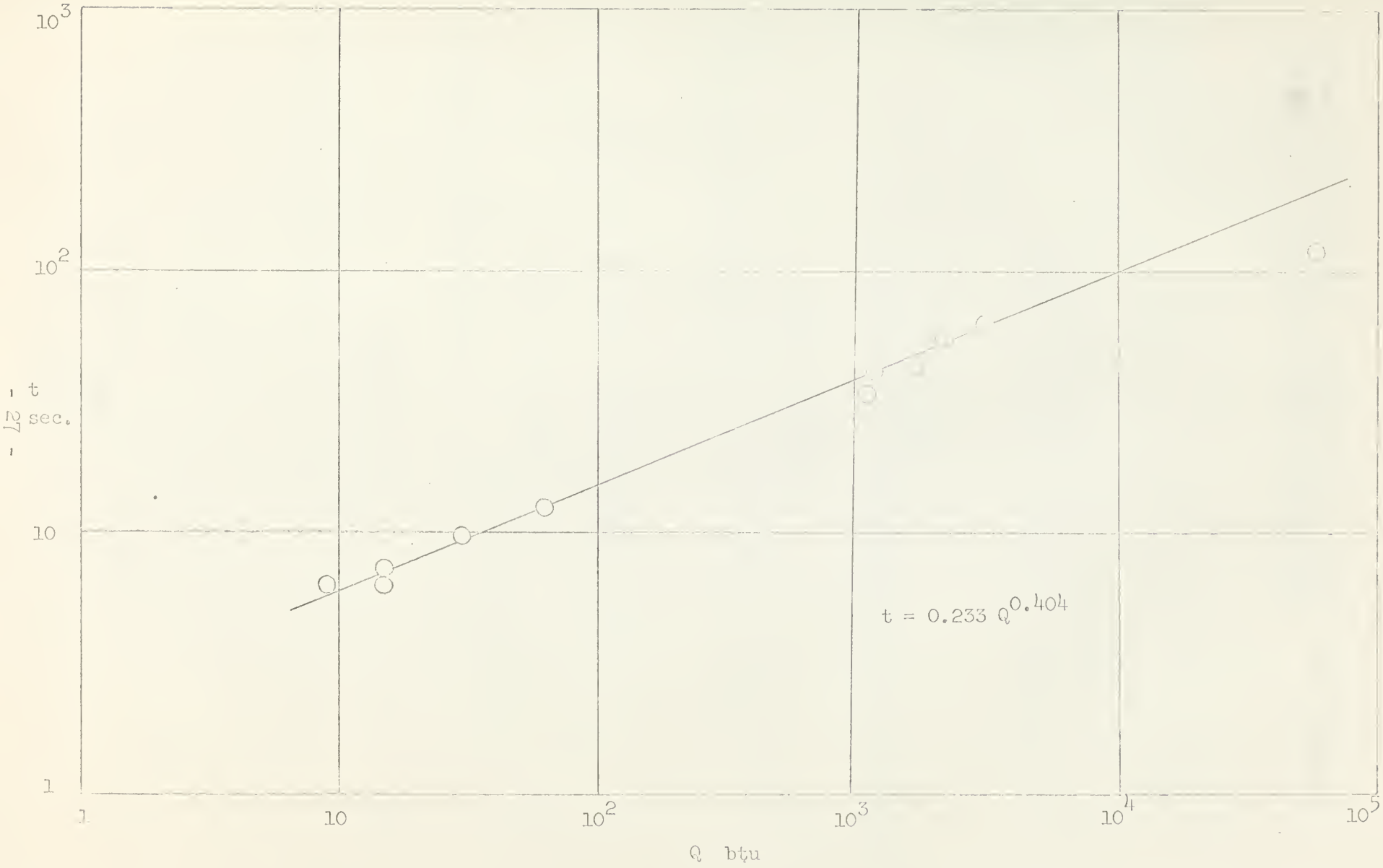

Fig. 15 HEAT ENERGY - CRITICAL TIME RELATION

IV THEORY

4.1 Basic Assumptions

The annulus is perfectly flat, of uniform thickness, homogeneous and perfectly elastic material, uniform temperature, and free from stresses in its initial state. The ratio h/b is very small compared to unity and therefore a condition of plain stress exists. Edge conditions and temperature distribution remain perfectly axisymmetric and the effect of gravity forces can be neglected. Small deflection theory is assumed.

4.2 General Thermal Stress Equations

From the theory of elasticity[1,4] the basic equilibrium equation is

$$\frac{\partial \sigma_r}{\partial r} + \frac{\sigma_r - \sigma_\theta}{r} = 0 \tag{1}$$

the stress-strain relations are

$$\epsilon_r - \alpha T = \frac{1}{E}(\sigma_r - \nu\sigma_\theta)$$

$$\epsilon_\theta - \alpha T = \frac{1}{E}(\sigma_\theta - \nu\sigma_r) \tag{2}$$

and with the radial displacement u

$$\epsilon_r = \frac{du}{dr}, \quad \epsilon_\theta = \frac{u}{r} \tag{3}$$

Solving (2) for the stresses

$$\sigma_r = \frac{E}{1-\nu^2}\left[\epsilon_r + \nu\epsilon_\theta - (1+\nu)\alpha T\right]$$

$$\sigma_\theta = \frac{E}{1-\nu^2}\left[\epsilon_\theta + \nu\epsilon_r - (1+\nu)\alpha T\right] \tag{4}$$

Substituting in equation (1)

$$r \frac{d}{dr} (\epsilon_r + \nu\epsilon_\theta) + (1-\nu)(\epsilon_r - \epsilon_\theta) = (1+\nu)\, r\alpha \frac{\partial T}{\partial r} \qquad (5)$$

and replacing strain by the functions given in (3)

$$\frac{d^2u}{dr^2} + \frac{1}{r}\frac{du}{dr} - \frac{u}{r^2} = (1+\nu)\,\alpha \frac{\partial T}{\partial r} \qquad (6)$$

Integrating both sides twice

$$u = \frac{(1+\nu)}{r}\,\alpha \int_a^r rTdr + c_1 r + \frac{c_2}{r} \qquad (7)$$

where c_1 and c_2 are constants of integration. Substituting (7) into (3) and the results into (4) gives the general equations

$$\sigma_r = -\frac{\alpha E}{r^2} \int_a^r Trdr + \frac{E}{1-\nu^2}\left[c_1 (1+\nu) - \frac{c_2}{r^2}(1-\nu)\right] \qquad (8)$$

$$\sigma_\theta = \frac{\alpha E}{r^2} \int_a^r Trdr - \alpha E T + \frac{E}{1-\nu^2}\left[c_1 (1+\nu) + \frac{c_2}{r^2}(1-\nu)\right] \qquad (9)$$

4.3 Thermal Stress Equations for Free Edge Condition

The boundary conditions for the free edge case are

$$(\sigma_r)_{r=a} = 0 \,, \quad (\sigma_r)_{r=b} = 0$$

Applying the conditions to equation (8) and subtracting

$$c_2 = \frac{a^2\alpha(1+\nu)}{b^2 - a^2} \int_a^b Trdr$$

hence

$$c_1 = \frac{\alpha(1-\nu)}{b^2 - a^2} \int_a^b Trdr$$

Substituting in equations (8) and (9)

$$\sigma_r = \frac{\alpha E}{r^2}\left[\frac{r^2 - a^2}{b^2 - a^2} \int_a^b Trdr - \int_a^r Trdr\right] \qquad (10)$$

$$\sigma_\theta = \frac{\alpha E}{r^2}\left[\frac{r^2 + a^2}{b^2 - a^2} \int_a^b Trdr + \int_a^r Trdr - Tr^2\right] \qquad (11)$$

4.4 Thermal Stress Equations for Fixed Edge Condition

The boundary conditions for the fixed edge case are

$$(\sigma_r)_{r=a} = 0 \ , \quad (u)_{r=b} = 0$$

Substituting in equation (3) and solving

$$c_1 = -\frac{\alpha(1-\nu)^2}{b^2(1-\nu) + a^2(1+\nu)} \int_a^b Trdr$$

$$c_2 = -\frac{\alpha a^2(1+\nu)^2}{b^2(1-\nu) + a^2(1+\nu)} \int_a^b Trdr$$

Substituting in equations (8) and (9)

$$\sigma_r = -\frac{\alpha E}{r^2}\left[\frac{(r^2-a^2)(1+\nu)}{b^2(1-\nu)+a^2(1+\nu)}\int_a^b Tr\,dr + \int_a^r Tr\,dr\right] \qquad (12)$$

$$\sigma_\theta = -\frac{\alpha E}{r^2}\left[\frac{(r^2+a^2)(1+\nu)}{b^2(1-\nu)+a^2(1+\nu)}\int_a^b Tr\,dr - \int_a^r Tr\,dr + Tr^2\right] \qquad (13)$$

4.5 The Differential Equation for Buckling

From the theory of plates[5] the differential equation for a deflected plate is

$$\nabla^4 w = \frac{q}{D} \qquad (14)$$

where

$$D = \frac{Eh^3}{12(1-\nu^2)}$$

and

$$\nabla^2 w = \frac{\partial^2 w}{\partial r^2} + \frac{1}{r}\frac{\partial w}{\partial r} + \frac{1}{r^2}\frac{\partial^2 w}{\partial \theta^2}$$

In the plain stress problem under consideration there are no external loads normal to the plate. However, when buckling occurs the thermal loads in the plane of the annulus are slightly tilted and hence yield vertical components.

A typical plate element is shown in Fig.13. The forces are assumed to act in the middle plane of the element and along the arc $\overline{AB}$ the force is $h\sigma_r r\,d\theta$. However, the force is tilted by the small angle $\frac{\partial w}{\partial r}$ so that the vertical component is $h\sigma_r r d\theta \frac{\partial w}{\partial r}$. Considering the arc shifted outward by an amount dr an analogous component is acting on $\overline{CD}$. The force $h\sigma_\theta dr$ acts along the side $\overline{AC}$ and is

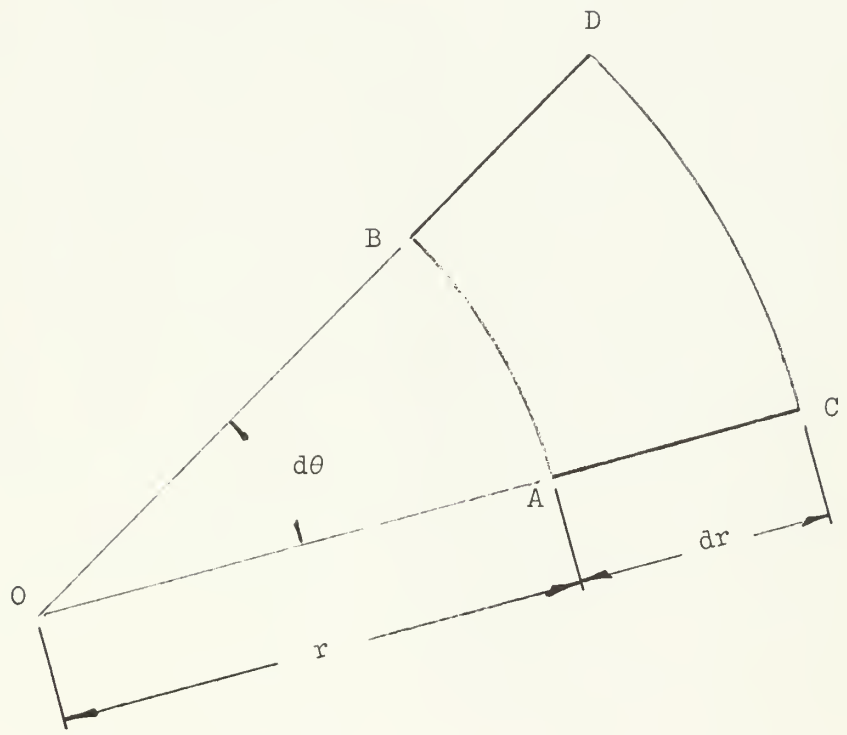

Fig. 16 TYPICAL RING ELEMENT

tilted by the angle $\frac{1}{r}\frac{\partial w}{\partial \theta}$, hence the vertical component is $\frac{h}{r}\sigma_\theta dr\frac{\partial w}{\partial \theta}$. Considering the radial shifted through an angle $d\theta$ an analogous component is acting on $\overline{BD}$. The resultant vertical force acting on the element $\overline{ABCD}$ is given by

$$\left(h\sigma_r r\frac{\partial w}{\partial r}\right)_{r+dr} d\theta - \left(h\sigma_r r\frac{\partial w}{\partial r}\right)_r d\theta + \left(\frac{h}{r}\sigma_\theta\frac{\partial w}{\partial \theta}\right)_{\theta+d\theta} dr - \left(\frac{h}{r}\sigma_\theta\frac{\partial w}{\partial \theta}\right)_\theta dr$$

or

$$h\frac{\partial}{\partial r}\left(\sigma_r r\frac{\partial w}{\partial r}\right)drd\theta + \frac{h}{r}\frac{\partial}{\partial \theta}\left(\sigma_\theta\frac{\partial w}{\partial \theta}\right)drd\theta$$

Dividing by $rd\theta dr$, the area of the element, yields the specific vertical load

$$q = \frac{h}{r}\frac{\partial}{\partial r}\left(\sigma_r r\frac{\partial w}{\partial r}\right) + \frac{h}{r^2}\frac{\partial}{\partial \theta}\left(\sigma_\theta\frac{\partial w}{\partial \theta}\right)$$

Substituting into equation (14)

$$\nabla^4 w = \frac{h}{Dr^2}\left[r\frac{\partial}{\partial r}\left(\sigma_r r\frac{\partial w}{\partial r}\right) + \frac{\partial}{\partial \theta}\left(\sigma_\theta\frac{\partial w}{\partial \theta}\right)\right] \qquad (15)$$

which is the general equation for the deflection w . However, for the axisymmetric case, this can be simplified to

$$\frac{1}{r}\frac{d}{dr}\left\{r\frac{d}{dr}\left[\frac{1}{r}\frac{d}{dr}\left(r\frac{dw}{dr}\right)\right]\right\} = \frac{h}{Dr}\frac{\partial}{\partial r}\left(\sigma_r r\frac{\partial w}{\partial r}\right)$$

Letting $\zeta = \frac{\partial w}{\partial r}$ and integrating

$$r\frac{d}{dr}\left[\frac{1}{r}\frac{d}{dr}(r\zeta)\right] = \frac{h}{D}\sigma_r r\zeta + c$$

or

$$\frac{\partial^2 \zeta}{\partial r^2} + \frac{1}{r}\frac{\partial \zeta}{\partial r} - \frac{1}{r^2}\zeta = \frac{h}{D}\sigma_r \zeta + \frac{c}{r}$$

where c is a constant of integration. In the special case under consideration where the inner edge is always free, the moment and shear force must be zero, consequently the constant c is zero. Therefore, the differential equation for buckling is

$$\frac{\partial^2 \zeta}{\partial r^2} + \frac{1}{r}\frac{\partial \zeta}{\partial r} - \left(\frac{1}{r^2} + \frac{h}{D}\sigma_r\right)\zeta = 0 \qquad (16)$$

For the outer edge clamped the boundary conditions become

$$(\zeta)_{r=b} = 0 \qquad (M)_{r=a} = -D\left(\frac{\partial \zeta}{\partial r} + \nu\frac{\zeta}{r}\right)_{r=a} = 0$$

For the outer edge free the boundary conditions are

$$0 = \left(\frac{\partial \zeta}{\partial r} + \nu\frac{\zeta}{r}\right)_{r=a} \qquad 0 = \left(\frac{\partial \zeta}{\partial r} + \nu\frac{\zeta}{r}\right)_{r=b}$$

It is well known that this equation is not readily solvable.

V CONCLUSIONS

In the tests on an annular plate described in this paper the temperature distribution achieved was in the form of a rectangular hyperbola. Under these conditions it is shown that the buckling coefficient can be described by the following equation

$$k = \frac{\alpha T_o}{h^2} \frac{(b^2 - a^2)}{(1-\nu^2)}$$

Moreover, it is demonstrated that the critical temperature and the time of buckling can be related to the increase in heat energy by the following equations

$$T_o = 2.95\, Q^{0.564}$$

$$t = 0.233\, Q^{0.404}$$

APPENDIX I

The following is the text of a paper presented by D. W. Mathews in Los Angeles, California, on May 12, 1961, to the Eleventh Annual Western Region Student Conference of the Institute of the Aerospace Sciences.

AN OPTICAL METHOD FOR THE DETERMINATION OF BUCKLING DEFLECTIONS

by

Lt.Col. W. B. Higgins, USMC

and

Lt. D. W. Mathews, USN

Stanford University
Stanford, California

INTRODUCTION

Success in experimental research depends upon the ability to measure length, time, and mass with precision. Thus over the years, much thought has been devoted by experimentalists to techniques for determining these quantities. Optical methods have long been accepted as the most precise for the determination of the flatness or shape of an object. Therefore, all engineers are acquainted with the principles of interferometery, the diffraction grating and the use of the optical comparator.

The structural problem with which we have been concerned is the determination of time of buckling and mode, in a plate heated in its center. It is clear, in a problem of this kind, that the means of measurement should not influence the results of the experiment.

Thus in our planning, many kinds of transducers or methods were considered, but in each case we found that there was an inter-action between transducer and the plate. Among the types of transducers we considered were: capacity type, gages, variable reluctance pick-ups and

---

The research outlined in this paper was sponsored by the United States Air Force under contract no. AF49(638)-223, and was carried out in the Department of Aeronautical Engineering at Stanford University under the direction of Professor W. H. Horton.

also linear potentiometers. They were all discarded in favor of an optical method. Clearly, a straight modification of the basic interferometric principle used for the determination of flatness is not possible, because the heat would cause the optical flats normally used on this type of work, to distort and so would interfere with our results. But the "Moire" pattern to be described in this paper does not have this disadvantage, nor indeed does it in any way interfere with the problem.

As we shall show, the method is extremely simple, accurate, low in cost, and readily available in any research laboratory. Indeed, the phenomenon has been observed by us all, usually without appreciating its significance. Most of us have noticed that the overlapping of two lattices of nearly equal mesh produces visible fringe patterns when viewed against a light background. Because this effect is merely mechanical, and is not related to the nature of the light employed, it is convenient to refer to it as mechanical interference. It is the purpose of this paper, to investigate the possible uses of this phenomenon in connection with the determination of the buckling of plates.

GENERAL

When a uniform set of parallel lines, produced on a transparent material, is superposed on another set of identical lines and moved in a direction normal to them, we get alternate light and dark lines (fig.1). This variation is produced as the two sets of lines alternately overlap and interlap and is strictly a mechanical effect. If the spacing of one set of lines differs slightly from the other, the alternate areas of light and dark occur without relative movement (fig.2). The dark areas parallel to the lines are interference fringes.

Fringes are also visible when a set of parallel lines, produced on a transparent material, is superposed on another set of parallel lines at a slight angle (fig.3). The greater the angle between the sets of lines, up to a limit of ninety degrees, the greater the number of fringes.

Fig. 1

Fig. 2

Fig. 3

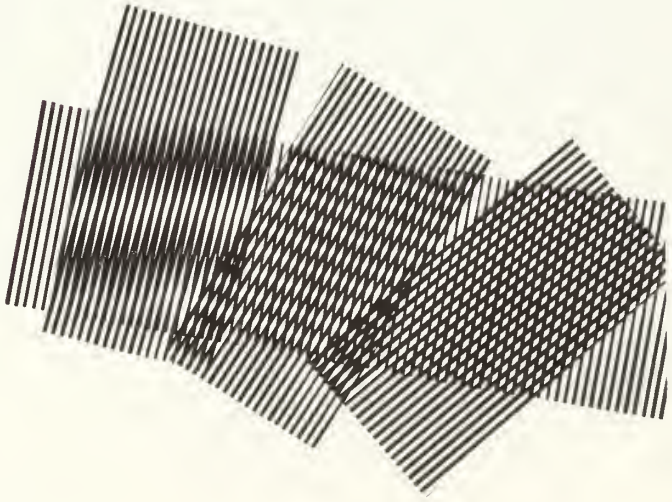

FRINGE PHENOMENON

For small angles, the fringes are at almost right angles to the lines. The relation being given as $90^{\circ} \pm \frac{\beta}{2}$ where β is the angle between the sets of lines. If h is the line spacing, the fringe spacing is $\frac{h}{2}$ cosecant $\frac{\beta}{2}$. This type of mechanical interference is known as "Moire" fringes; the name coming from the French and meaning: "having a wavelike pattern".

The physics of the method is extremely simple, it is nothing more than the reflection of a ray of light from a surface (fig.4). The change in angle of reflection is twice the change in angle of the reflecting surface. If the deflection of a reflected light ray is measured at a known distance, the change in slope of the surface can be calculated from geometry. As a simple expedient in bookkeeping of the rays, we use movement in one direction and alternate the color of the rays in that direction. In our case we use alternating black and white parallel lines. Sensitivity of the system can be increased by measuring movement of the associated "Moire" fringes. The sensitivity is directly proportional to the cotangent of the angle of rotation between the two sets of superposed lines.

The method is not new. It was first reported in 1948 by Weller and Shepard of the Naval Ordnance Laboratory, Washington, D.C. Their short paper described some of the possibilities of the method. It was followed in 1955 by a paper given by Ligtenberg from the Technological University of Delft. This paper was titled "The Moire Method - A New Experimental Method for the Determination of Moments in Small Slab Models". Ligtenberg placed a model with a mirror surface in front of a circular screen on which was ruled six lines per inch. From the center of the back of the screen, he viewed the reflected lines shown in the mirrored surface. Using a camera, he recorded the initial position of the reflected lines. The model was then loaded in such a manner that the deflections were normal to the screen and hence the change in slopes of the model surface caused the reflected lines to appear in a different position. A second exposure was superposed on the same film and consequently after development, "Moire" fringes appeared. From geometry, slopes of the model were calculated.

LIGHT RAY REFLECTION

Fig. 4

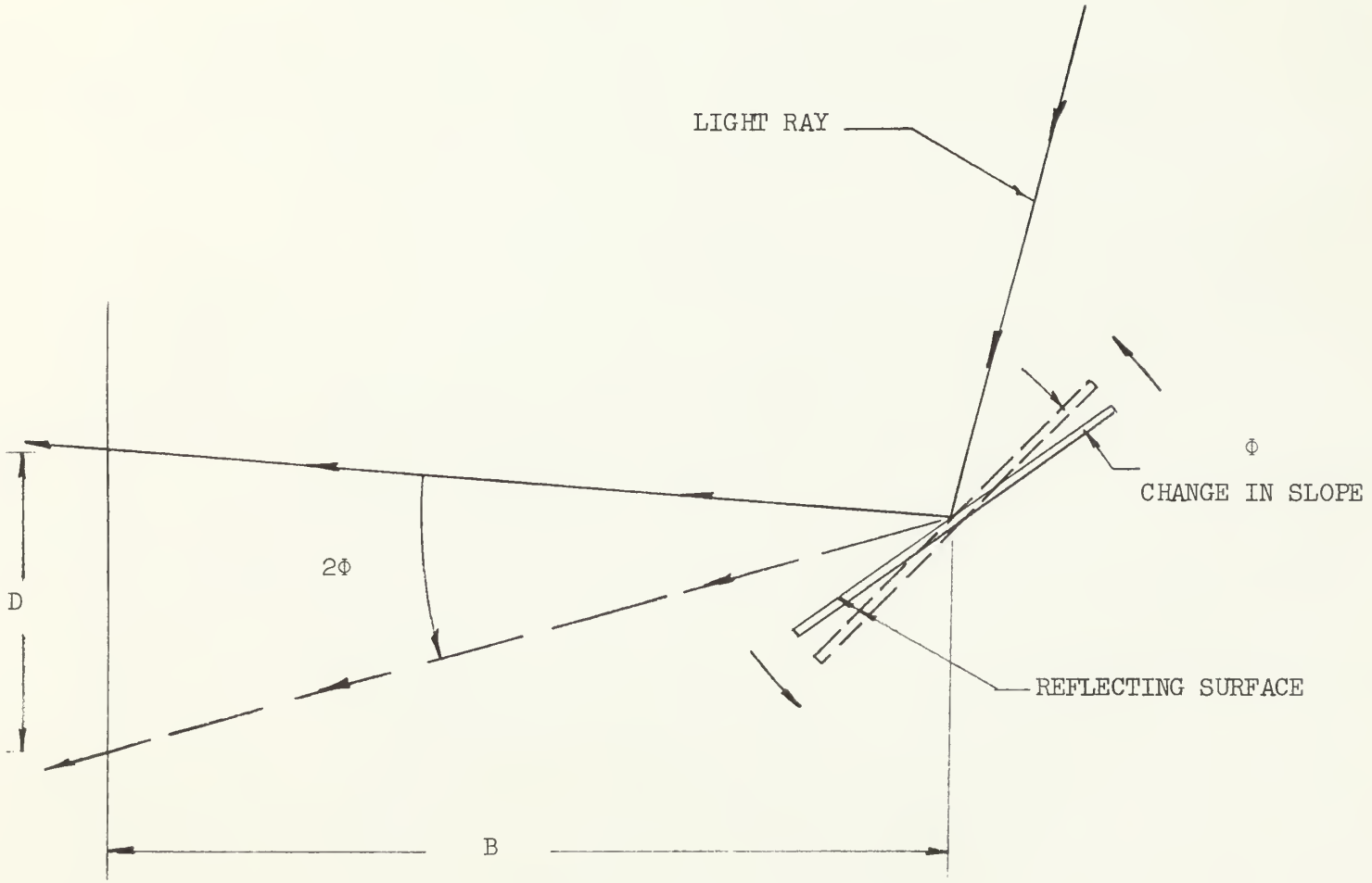

DEVELOPMENT

In order to develop a satisfactory procedure for measuring buckling deflections in the thermal stress problem, work was divided into three stages:

1. Development of the basic optical and photographic techniques.
2. Application of the techniques to a flat plate simply supported on two edges.
3. Actual application to the thermal stress problem involving a thin disc.

The first stage: A polaroid land camera was used to make a lantern slide transparency of a set of ruled parallel lines. Line and spacing width was one-sixteenth of an inch. A 35 mm slide made from the transparency was projected on a 10 × 12 inch alzac test surface with a La Belle 500 projector. The image of the lines was reflected from the test surface to a 20 × 20 × 1/8 inch milk glass focusing plate. The optics and equipment were symmetrically placed with respect to a horizontal plane, with the parallel lines and supporting edges of the test plate also horizontal (fig.5). This orientation provided maximum intensity and contrast because of the surface condition of the test plate. In manufacture of the alzac, minute scratches were made on the surface in line with the direction of rolling. These caused diffusion of the reflected light. With the projected lines oriented at right angles to the scratches, the diffusion of light reinforced the lines and hence intensity and contrast were at a maximum.

The second system of parallel lines was formed by placing paper strips across the back side of the milk glass, inclined by about ten degrees to the reflected horizontal lines. The optical distance of five feet produced lines of approximately three-sixteenths of an inch wide. Intensities of the two sets of lines were matched by varying the density of the paper strips. The "moire" fringe lines which appeared on the milk glass were successfully photographed with a Speed Graphic Camera (fig.6).

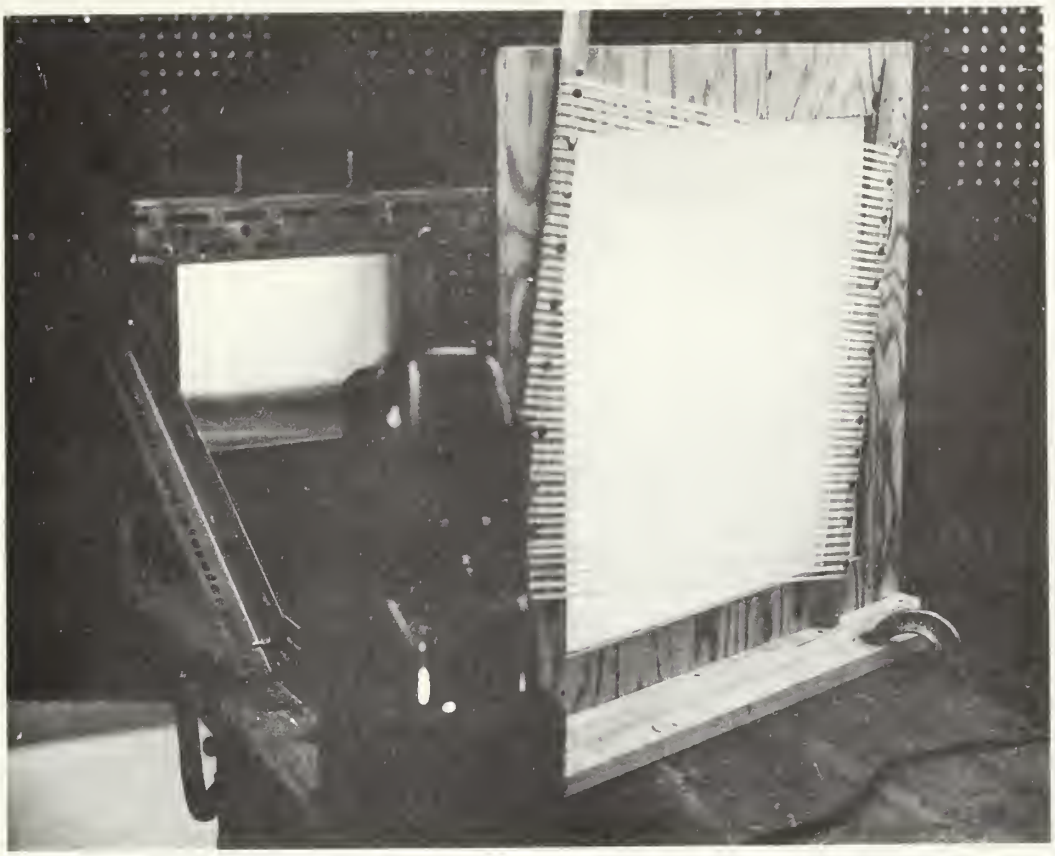

Fig.5 FIRST STAGE APPARATUS

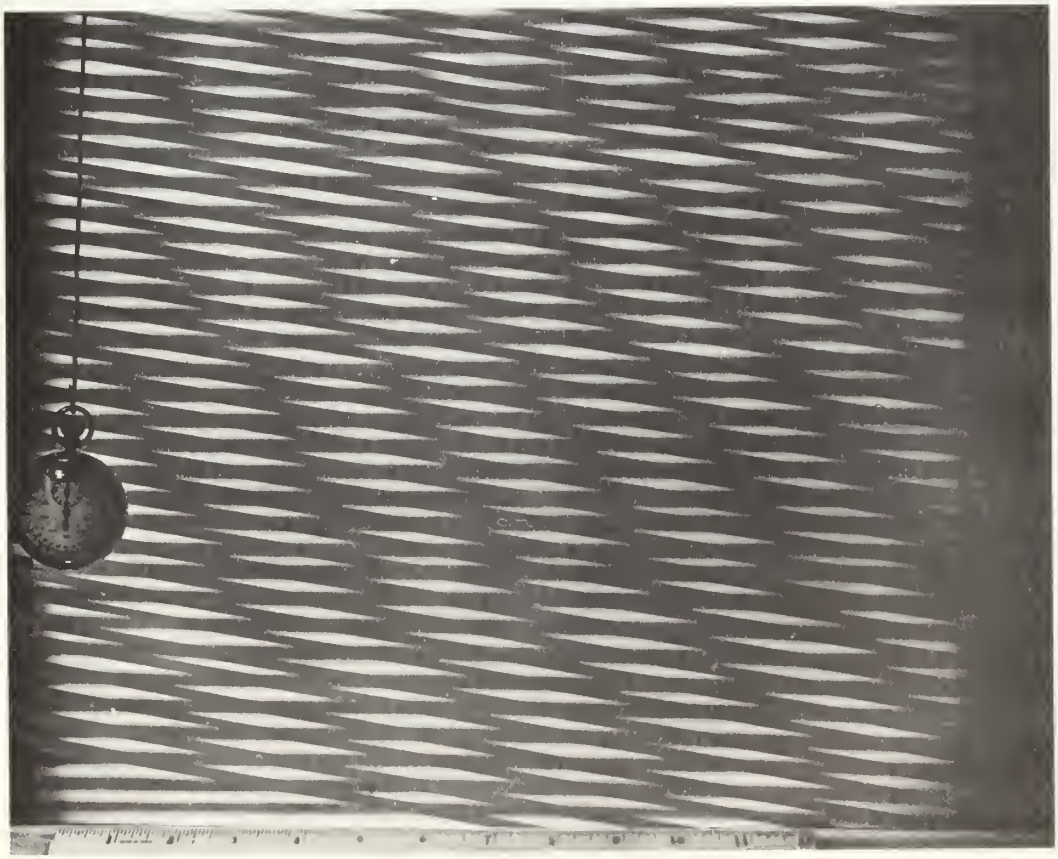

Fig.6 FIRST STAGE FRINGE PATTERN

It was found that the accuracy of the line spacing was most important in order to produce smooth fringes. Drafting tools were used to rule the set of lines photographed in this test, but the uniformity of spacing was not the best. It was also found that more lines per inch were necessary to eliminate the jagged appearance of the fringes.

In the second stage, the geometry of the optics in the simply supported plate problem was as shown in figure 7. Two assumptions were made in our analysis. Delta is much less than B and $\tan 2\Phi$ is much less than one. Since the deflection of the plate is of the order of one-tenth of an inch and B is of the order thirty inches, delta can be neglected. The movement of the projected lines on the focusing plate is a function of the angle α, which varies for each line. The angle α corresponding to any projected line can be obtained from geometry. The maximum value for $\tan \alpha$ is 0.15 and for fringe movements up to about 25 inches, the error in assuming $\tan \alpha \tan 2\Phi$ equal to zero is less than 1%. Therefore, the equation reduces to $D = B \tan 2\Phi$ and a solution for the slope Φ for any observed line displacement is obtainable.

One main advantage of this method of measurement lies in the sensitivity which is gained by measurement of the relatively large movement of the fringe Γ for small movement of the reflected line D. The slope at a distance x from the origin is therefore determined from the equation $\tan 2\Phi = \frac{\Gamma}{B} \tan \beta$.

To demonstrate the sensitivity, three central deflections were used at the one-quarter point of the test specimen. The angle between the sets of lines being 10 degrees. For a central deflection of one-tenth of an inch, the fringe movement corresponding to the change in slope at the one-quarter point was 7 inches. For a deflection of one one-hundredth, the fringe movement was approximately three quarters, and a one one-thousandth, a sixteenth. The high sensitivity achieved with this method is evident.

The development is now in the third stage and is based on the following proposal (fig.8). In the actual experiment, temperature and deflection will be recorded versus time from the instant the heat source is turned on until thermal equilibrium is reached. A motion picture camera will be

GEOMETRY

Fig. 7

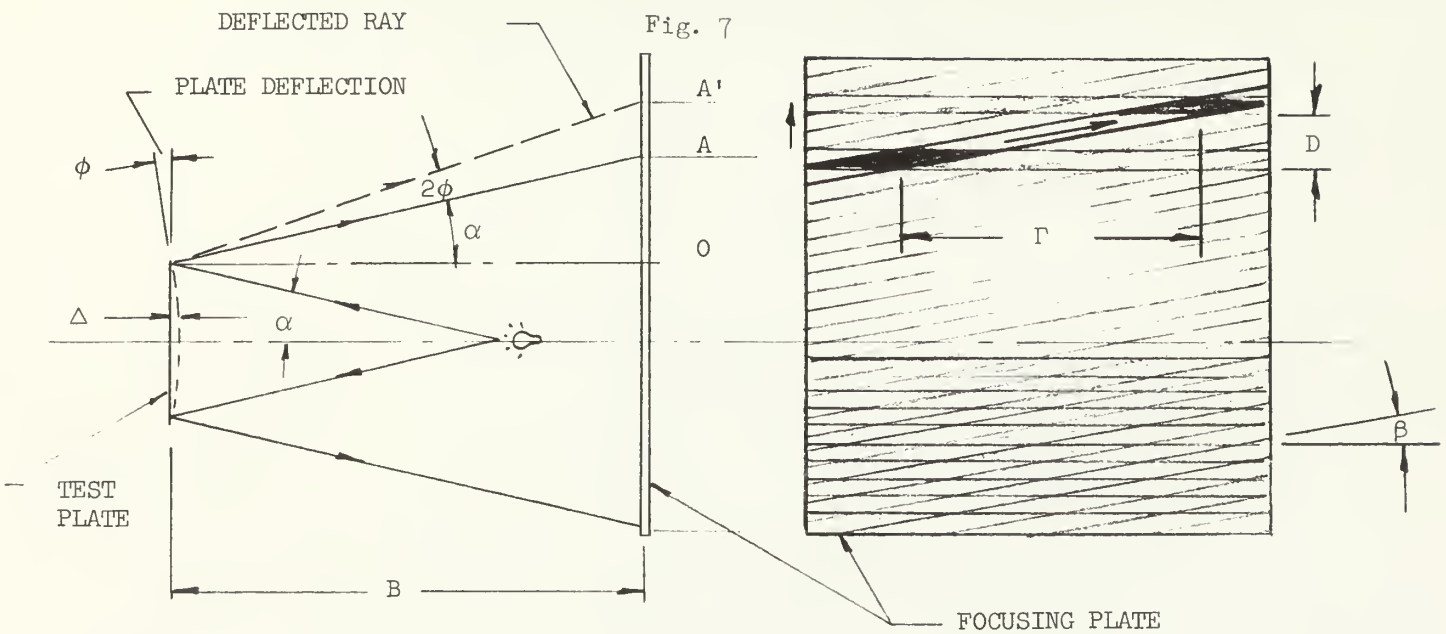

FROM GEOMETRY: $D = OA' - OA = (B - \Delta)[\tan(2\phi + \alpha)] - B \tan \alpha$

$$= (B - \Delta)\left[\frac{\tan 2\phi + \tan \alpha}{1 - \tan \alpha \tan 2\phi}\right] - B \tan \alpha$$

ASSUMPTIONS: 1. $\Delta \ll B$, 2. $\tan \alpha \tan 2\phi \ll 1$

THEREFORE: $D = B \tan 2\phi$ BUT $\tan \beta = D/\Gamma$

THEREFORE:

$$\tan 2\phi_x = \frac{\Gamma_x}{B} \tan \beta$$

PROPOSED SYSTEM

Fig. 8

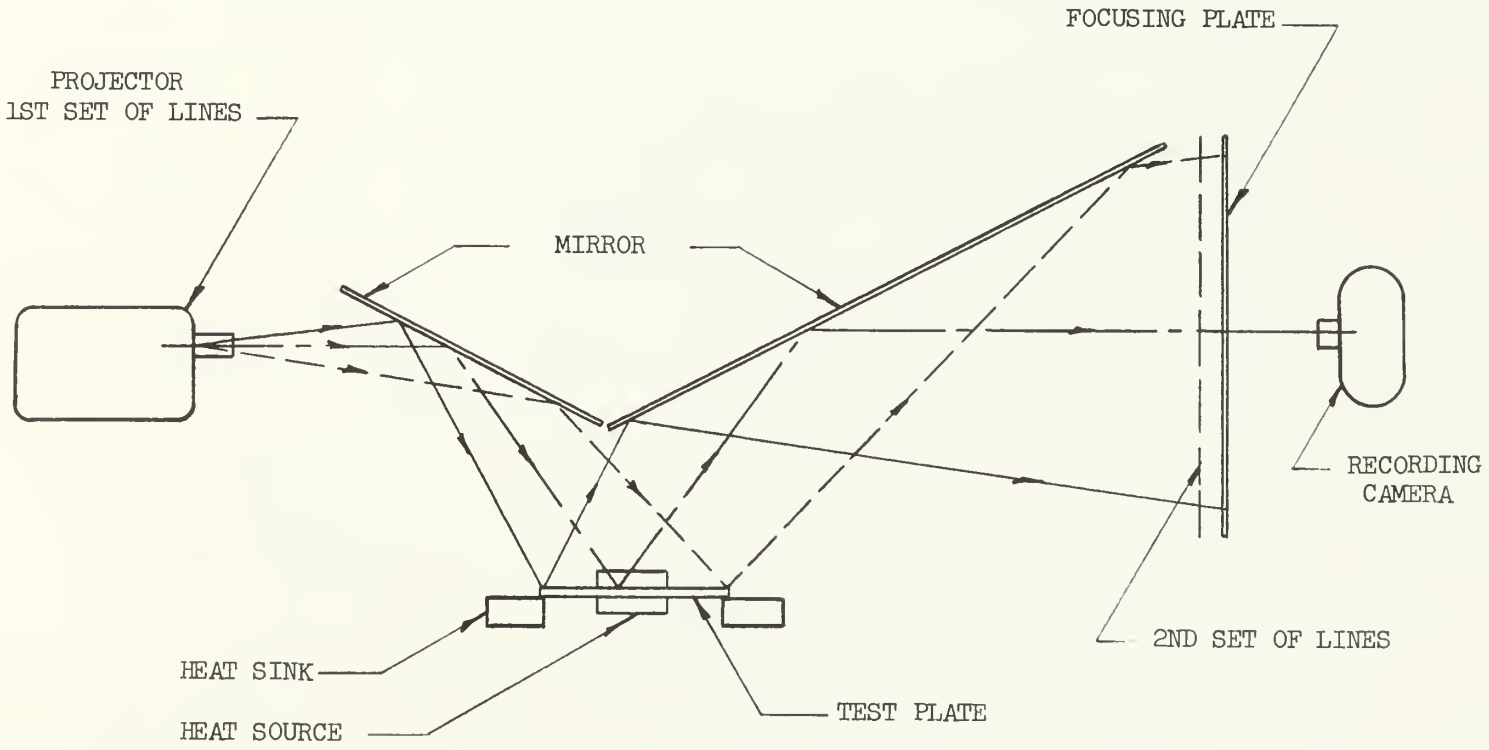

used to record changing position of the fringes. A stop watch and scales will be included in the photograph to indicate the time on each frame of the film and establish the magnitude of fringe movement. The determination of time of initial buckling is simply determined by noting when movement of the fringe is apparent in the developed film. The actual movement of the fringes can be read by enlarging the appropriate frame for any given time, to a convenient size.

In testing the thermally stressed disc, it was desired to mount the disc in a horizontal position, therefore, two plate glass mirrors were used to reflect the light rays to a more convenient position.

In preparing the slides for the final test, it was found that cellophane tape was available in widths of one-sixteenth of an inch and larger and in a variety of colors. The tape is sold under the trade name of Applied Graphics Corporation Drafting Tape.

A very precise set of parallel lines was constructed using three thirty-seconds tape, on frosted glass. This width was convenient to work with and the glass made it easy to adjust the tape. The use of tape also gave maximum definition to the line edge.

One of the problems with the earlier black and white lines was locating on the focusing plate, a point corresponding to a specific point on the test surface. A particular line could be traced through the optical system but because of the nature of the pattern, the lines soon begin to interchange and were difficult to follow. The new set was made using colored lines alternating black, green, red and blue. The lines, laid out in a fifteen inch square on the frosted glass, were photographed with a speed graphic camera using strobe illumination. The second set of lines was constructed with a spacing of thirty-six lines per foot by making a positive from a black and white negative. DuPont "Cronar", a dimensionally stable, high contrast litho film was used for the positive and is available in 22 × 29 inch sheets. The positive was sprayed with "Quik-Stick", a spray adhesive, on the emulsion side and simply stuck to the two and one-half foot square milk glass focusing plate.

A LaBelle 500 projector is used to project the two by two slides oriented with the lines vertical, to eliminate problems caused by the double image from the first surface of the mirror. In other words, the lines are simply reinforced by their own image.

The set of lines is reflected from the first mirror to the reflecting surface of the alzac test disc, then to the second mirror and finally through the second set of lines onto the milk glass. From the opposite side of the focusing plate, the individual lines and "Moire" fringes are clearly visible. Figure 9 illustrates the fringe pattern before buckling and figure 10 shows the fringes after buckling. The figures were taken from a 16 mm movie of a test run. The fringe movement is converted to slope using the derived formula and deflection obtained by graphical integration of the slope function.

CONCLUSIONS

In conclusion I would like to say, while further development is clearly required, we believe that this presentation of the "Moire" method has demonstrated that it is possible to determine the time of buckling of a loaded body with precision, that it is feasible to determine the mode of buckling over a relatively large area and that the equipment needed for such investigation is simple, inexpensive and readily available. Since contact with the object under investigation is totally unnecessary, the method can be applied in cases in which environmental conditions or interaction problems make the use of normal instrumentation either extremely difficult or not applicable.

It is important to point out that changes in deflection are derived from changes in slope, and therefore the technique is not restricted to initially plane surfaces or unloaded specimens.

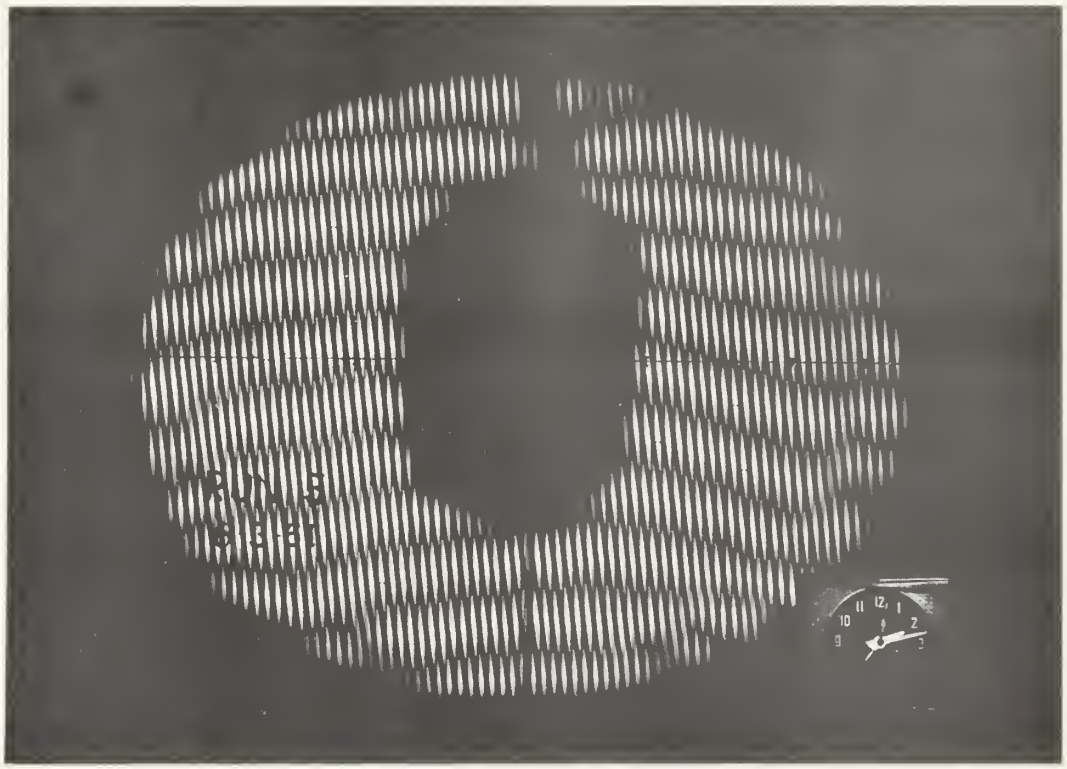

Fig.9 FRINGE PATTERN BEFORE BUCKLING

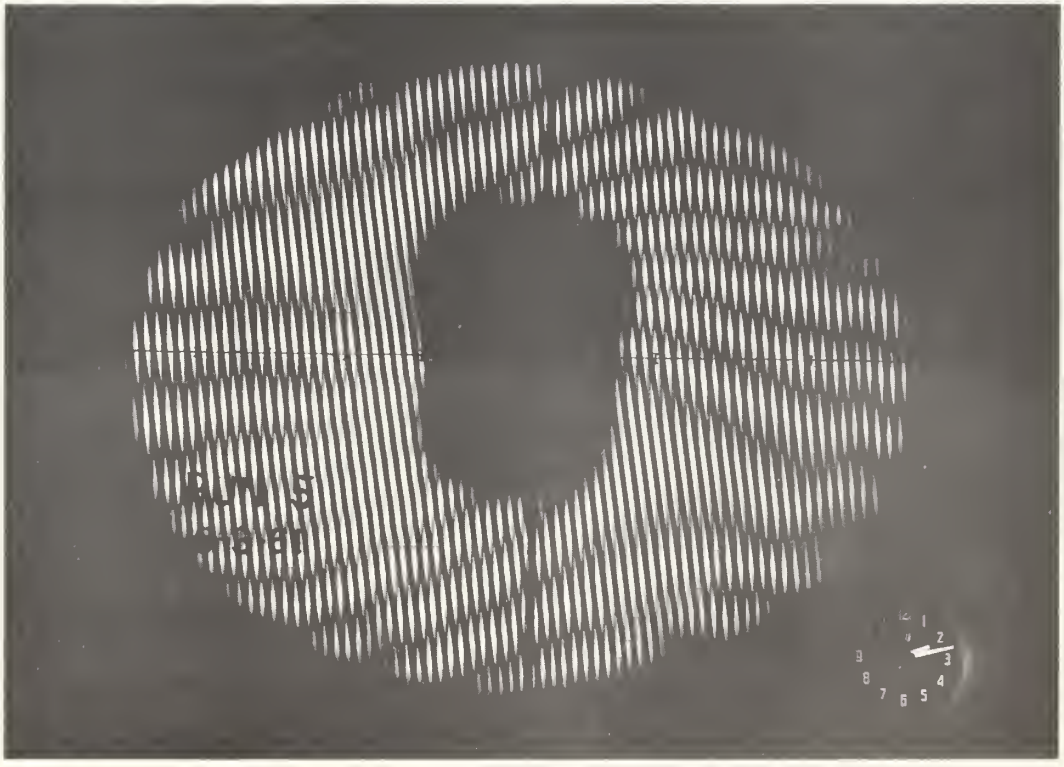

Fig.10 FRINGE PATTERN AFTER BUCKLING

BIBLIOGRAPHY

1. Displacement Measurement by Mechanical Interferometry, Weller, R., and Shepard, B. M., Society of Experimental Stress Analysis Proceedings, Vol.6, No.1.

2. The Moire Method - A New Experimental Method for the Determination of Moments in Small Slab Models, Ligtenberg, F. K., Society of Experimental Stress Analysis Proceedings, Vol.12, No.2.

APPENDIX II

SAMPLE CALCULATIONS

The reduction of data and subsequent calculations for run 29 were obtained in the following manner. Galvanometer deflection at buckling was measured in units of the Oscillogram Reader. The corresponding millivoltage was then obtained using a curve plotted from a calibration run. After a correction for the room temperature reference junction was made, standard Leeds and Northrup Conversion Tables were used to find temperature in degrees fahrenheit. For this case room temperature was 74.5°F, therefore a correction of 0.94 millivolts was added to the galvanometer voltage. Subtracting room temperature gave the desired rise T. Values are shown in Table III. Temperature rise versus radius are shown in Fig.1. Integration of $\int_a^r rTdr$ was completed graphically by plotting the function rT and measuring the area under the curve with a planimeter. See Fig.2.

A typical calculation of the stress parameter is shown for $r = 1.825$ in. From equation (10)

$$\sigma_r = \frac{\alpha E}{r^2}\left[\frac{r^2 - a^2}{b^2 - a^2}\int_a^b Trdr - \int_a^r Trdr\right]$$

or dividing both sides by T_o and defining $\tau = \frac{T}{T_o}$

$$H = \frac{\sigma_r}{T_o \alpha E} = \frac{1}{r^2}\left[\frac{r^2 - a^2}{b^2 - a^2}\int_a^b \tau rdr - \int_a^r \tau rdr\right]$$

Since $r = 1.825$ in., $a = 1.625$ in., $b = 6$ in., and from Fig.2

$\int_a^b \tau rdr = 0.135$ and $\int_a^{r=1.825} \tau rdr = 0.154$

$$H = \frac{1}{(1.825)^2}\left[\frac{(1.825)^2 - (1.625)^2}{(6)^2 - (1.625)^2}(0.185) - (0.154)\right] = 0.045$$

TABLE III

SAMPLE CALCULATION

RUN 29

Galvanometer number:	1	2	3	4	5	6	7	8
Galvanometer deflection:								
Oscillogram Reader Units	16	126	52	10	10	172	140	119
Millivolts	0.022	0.226	0.082	0.015	0.015	0.286	0.247	0.212
Temperature corrected to 32°F:								
Millivolts	0.962	1.166	1.022	0.955	0.955	1.226	1.187	1.152
Plate temperature:								
°F	75½	84½	78	75	75	87	85	84
Temperature rise T :								
°F	1	10*	3½	½	½	12½	10½	9½*
Thermocouple location:								
Inches from inner edge	0.250	0.040	0.125	0.500	0.375	0.010	0.010	0.030

* Two extra thermocouples were used on this run and the results are not shown in the summary of data

Fig. 1 RUN 29 - TEMPERATURE DISTRIBUTION AT BUCKLING

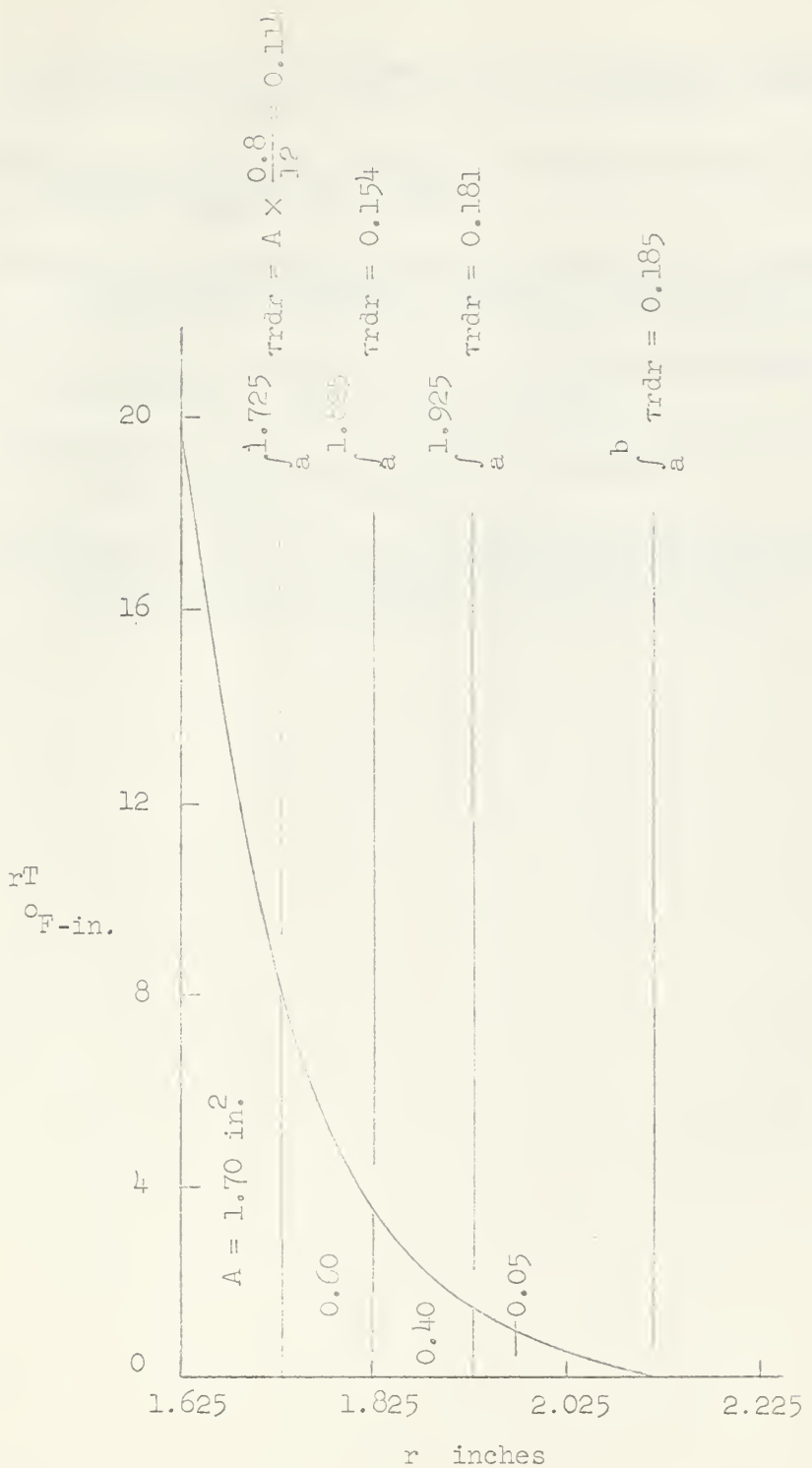

Fig. 2 RUN 29 - GRAPHICAL INTEGRATION

REFERENCES

1. Timoshenko, S., and Goodier, J. N.: Theory of Elasticity, 2nd ed., McGraw-Hill Book Co. Inc., New York

2. Queinec, A.: "Thermal Buckling of Centrally Heated Circular Plates", SUDAER No.106, June 1961

3. Holmes, M.: "Compression Tests on Thin-Walled Cylinders", The Aeronautical Quarterly, Vol.XII, Part 2, May 1961

4. Boley, Bruno A., and Weiner, J. H.: Theory of Thermal Stresses, John Wiley and Sons, Inc., New York

5. Timoshenko, S.: Theory of Elastic Stability, 1st ed., McGraw-Hill Book Co. Inc., New York

6. Meissner, E. T. H., "On the Buckling of Circular Discs", Schweizerische Bauzeitung, Vol.101, p.87, 1933

Lorna G. Smith
Aero. Eng'g. Dept.
Stanford University